MATLAB/SIMULINK IMPLEMENTATION AND ANALYSIS

OF THREE PULSE-WIDTH-MODULATION (PWM)

TECHNIQUES

by

Phuong Hue Tran

A thesis

submitted in partial fulfillment

of the requirements for the degree of

Master of Science in Electrical Engineering

Boise State University

May 2012

BOISE STATE UNIVERSITY GRADUATE COLLEGE

DEFENSE COMMITTEE AND FINAL READING APPROVALS

of the thesis submitted by

Phuong Hue Tran

Thesis Title: MATLAB/Simulink Implementation and Analysis of Three Pulse-Width-Modulation (PWM) Techniques

Date of Final Oral Examination: 11 May 2012

The following individuals read and discussed the thesis submitted by student Phuong Hue Tran, and they evaluated her presentation and response to questions during the final oral examination. They found that the student passed the final oral examination.

Said Ahmed-Zaid, Ph.D.   Chair, Supervisory Committee

Elisa Barney Smith, Ph.D.   Member, Supervisory Committee

John Chiasson, Ph.D.   Member, Supervisory Committee

The final reading approval of the thesis was granted by Said Ahmed-Zaid, Ph.D., Chair of the Supervisory Committee. The thesis was approved for the Graduate College by John R. Pelton, Ph.D., Dean of the Graduate College.

ACKNOWLEDGMENTS

I would like to take this opportunity to express my sincere appreciation to all the people who were helpful in making this thesis successful. First of all, I would like to express my gratitude to my advisor, Dr. Said Ahmed-Zaid for his valuable comments, guidance, and discussions that guided me well in the process of my thesis. I am thankful to my committee members (Dr. John Chiasson and Dr. Elisa Barney Smith) for their comments and suggestions and their willingness to be my committee members.

Most importantly, I would like to express my deepest thanks to my family for giving me a life of opportunities and backing me up in every corner where my life has been difficult. Thanks for all their care, support, encouragement, and inspiration all along in my academic endeavors.

ABSTRACT

With advances in solid-state power electronic devices and microprocessors, various pulse-width-modulation (PWM) techniques have been developed for industrial applications. For example, PWM-based three-phase voltage source inverters (VSI) convert DC power to AC power with variable voltage magnitude and variable frequency.

This thesis discusses the advantages and drawbacks of three different PWM techniques: the sinusoidal PWM (SPWM) technique, the third-harmonic-injection PWM (THIPWM) technique, and the space-vector PWM (SVPWM) technique. These three methods are compared by discussing their ease of implementation and by analyzing the output harmonic spectra of various output voltages (poles voltages, line-to-neutral voltages, and line-to-line voltages) and their total harmonic distortion (THD).

The simulation results show that both the THIPWM and SVPWM techniques have lower total harmonic distortion than the SPWM technique. The THIPWM and SVPWM techniques in the under-modulation region can both increase the fundamental output voltage by 15.5% over the SPWM technique. Moreover, the SVPWM technique can increase the fundamental output by about 5% in each of the overmodulation regions 1 and 2, respectively.

TABLE OF CONTENTS

LIST OF TABLES

LIST OF FIGURES

CHAPTER 1

INTRODUCTION

1.1   Introduction

Pulse-width modulation (PWM) is a technique where the duty ratio of a pulsating wave-form is controlled by another input waveform. The intersections between the reference voltage waveform and the carrier waveform give the opening and closing times of the switches.

PWM is commonly used in applications like motor speed control, converters, audio amplifiers, etc. For example, it is used to reduce the total power delivered to a load without losses, which normally occurs when a power source is limited by a resistive element. PWM is used to adjust the voltage applied to the motor. Changing the duty ratio of the switches changes the speed of the motor. The longer the pulse is closed compared to the opened periods, the higher the power supplied to the load is. The change of state between closing (ON) and opening (OFF) is rapid, so that the average power dissipation is very low compared to the power being delivered. PWM amplifiers are more efficient and less bulky than linear power amplifiers. In addition, linear amplifiers that deliver energy continuously rather than through pulses have lower maximum power ratings than PWM amplifiers.

There is no single PWM method that is the best suited for all applications and with ad-vances in solid-state power electronic devices and microprocessors, various pulse-width-modulation (PWM) techniques have been developed for industrial applications. For these reasons, the PWM techniques have been the subject of intensive research since 1970s.

1.2 Literature Review

With advances in solid-state power electronic devices and microprocessors, various inverter control techniques employing pulse-width-modulation (PWM) techniques are becoming increasingly popular in AC motor drive applications. These PWM-based drives are used to control both the frequency and the magnitude of the voltages applied to motors [1]. Various PWM strategies, control schemes, and realization techniques have been developed in the past two decades [2]. PWM strategy plays an important role in the minimization of harmonics and switching losses in converters, especially in three-phase applications. The first modulation techniques were developed in the mid-1960s by Kirnnich, Heinrick, and Bowes as reported in [3]. The research in PWM schemes has intensified in the last few decades. The main aim of any modulation technique is to obtain a variable output with a maximum fundamental component and minimum harmonics [4].

The carrier-based PWM methods were developed first and were widely used in most applications. One of the earliest modulation signals for carrier-based PWM is sinusoidal PWM (SPWM). The SPWM technique is based on the comparison of a carrier signal and a pure sinusoidal modulation signal. It was introduced by Schonung and Stemmler in 1964 as reported in [5]. The utilization rate of the DC voltage for traditional sinusoidal PWM is only 78.5% of the DC bus voltage, which is far less than that of the six-step wave (100%). Improving the utilization rate of the DC bus voltage has been a research focus in power electronics [6].

This problem of the under-utilization of the DC bus voltage led to the development of the third-harmonic-injection pulse-width modulation (THIPWM). In 1975, Buja developed this improved sinusoidal PWM technique, which added a third-order harmonic content into the sinusoidal reference signal leading to a 15.5% increase in the utilization rate of the DC bus voltage [6].

Another method of increasing the output voltage is the space-vector PWM (SVPWM)

technique. SVPWM was first introduced in the mid-1980s and was greatly advanced by Van Der Broeck in 1988 [9]. Compared to THIPWM, the two techniques have similar results but their methods of implementation are completely different. With the development of microprocessors, SVPWM has become one of the most important PWM methods for three-phase inverters [7]. Many SVPWM schemes have been developed and extensively investigated in the literature. The goal in each modulation strategy is to lower the switching losses, maximize bus utilization, reduce harmonic content, and still achieve precise control [8].

The SVPWM technique utilizes the DC bus voltage more efficiently and generates less harmonic distortion when compared with the SPWM technique [4]. The maximum peak fundamental magnitude of the SVPWM technique is about 90.6% of the inverter capacity. This represents a 15.5% increase in the maximum voltage compared with conventional sinusoidal modulation [10].

In 1991, Holtz proposed a classical over-modulation technique based on SVPWM, which divided the over-modulation range into two modes of operation and increased the utilization rate of the DC voltage to that of a six-step wave [6,11,12,13]. Holtz proposed this technique using switching time calculations in the over-modulation region of SVPWM.

In 1998, Lee analyzed Holtz's over-modulation technique graphically, gave some approximate linear expressions between the modulation index and its own auxiliary parameter, and discussed the harmonic problem [14]. He showed that this technique generated less harmonic distortion in the output voltages (or) the currents applied to the phases of an AC motor and provided more efficient use of the DC input voltage. Because of its superior performance characteristics, it has found widespread application in recent years [4]. Accordingly, many other researchers have explored various aspects of this technique in the literature [6,15,16,17].

1.3   Research Motivation

The SPWM technique is the easiest modulation scheme to understand and to implement in software or hardware but this technique is unable to fully utilize the DC bus supply voltage available to the voltage source inverter. This drawback led to the development of THIPWM and SVPWM. THIPWM is a technique that adds a third-order harmonic content to a sinusoidal reference signal thereby increasing the utilization rate of the DC bus voltage by 15.5%.

The implementation of the conventional SVPWM is especially difficult because it requires complicated mathematical operations. In the under-modulation region, this algorithm provides 15.5% higher output voltages compared to the SPWM technique. Moreover, the utilization of the DC bus voltage can be further increased when extending into the over-modulation region of SVPWM.

Three-phase voltage source pulse-width modulation inverters have been widely used for DC to AC power conversion since they can produce outputs with variable voltage magnitude and variable frequency. For example, modern power electronics controllers have been rapidly moving toward digital implementation. Typical solutions employ microcontrollers or DSPs [18].

This thesis discusses the principles, theories, mathematical equations, and procedures involved for the software (MATLAB/Simulink package) implementation of these techniques. This thesis synthesizes and compares the main theories behind three-phase generation of SPWM, THIPWM, and SVPWM. These three techniques are used to generate their respective output PWM signals, which are then compared based on harmonic content and distortion using the total harmonic distortion (THD) measure of various output voltages.

1.4   Thesis Organization

This thesis is comprised of seven chapters. Chapter 1 is an introduction including a literature review, research motivation, and thesis outline. Chapters 2, 3, and 4 provide an in-depth look into the concepts, mathematical equations, implementation, and waveforms generated by the SPWM, THIPWM, and SVPWM techniques. Chapter 5 presents the Simulink models and output plots obtained from the simulation of SPWM, THIPWM, and SVPWM in the under-modulation region and over-modulation region 1. Chapter 6 compares the results of these three techniques from Chapter 5 along with a discussion of the output harmonic spectra of various output voltages and a THD measure for each output. Chapter 7 summarizes the thesis with conclusions and recommendations for future research.

CHAPTER 2

SINUSOIDAL PWM AND THIRD-HARMONIC-INJECTION PWM

2.1 Sinusoidal PWM

2.1.1 Sinusoidal PWM Concept

The sinusoidal pulse-width modulation (SPWM) technique produces a sinusoidal waveform by filtering an output pulse waveform with varying width. A high switching frequency leads to a better filtered sinusoidal output waveform. The desired output voltage is achieved by varying the frequency and amplitude of a reference or modulating voltage. The variations in the amplitude and frequency of the reference voltage change the pulse-width patterns of the output voltage but keep the sinusoidal modulation.

As shown in Figure 2.1, a low-frequency sinusoidal modulating waveform is compared with a high-frequency triangular waveform, which is called the carrier waveform. The switching state is changed when the sine waveform intersects the triangular waveform. The crossing positions determine the variable switching times between states.

In three-phase SPWM, a triangular voltage waveform (V_T) is compared with three sinusoidal control voltages (V_a, V_b, and V_c), which are 120° out of phase with each other and the relative levels of the waveforms are used to control the switching of the devices in each phase leg of the inverter.

A six-step inverter is composed of six switches S_1 through S_6 with each phase output connected to the middle of each inverter leg as shown in Figure 2.2. The output of the comparators in Figure 2.1 form the control signals for the three legs of the inverter. Two
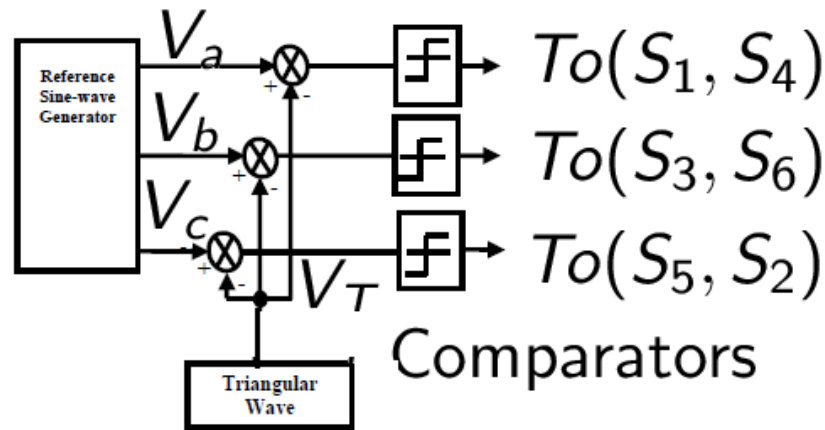
Figure 2.1: Control Signal Generator for SPWM [27].
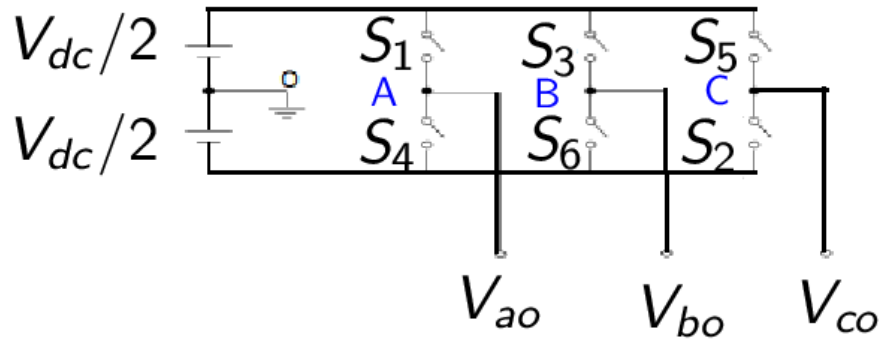
Figure 2.2: Three-Phase Sinusoidal PWM Inverter [27].

switches in each phase make up one leg and open and close in a complementary fashion. That is, when one switch is open, the other is closed and vice-versa. The output pole voltages V_{ao}, V_{bo}, and V_{co} of the inverter switch between $-V_{dc}/2$ and $+V_{dc}/2$ voltage levels where V_{dc} is the total DC voltage.

The peak of the sine modulating waveform is always less than the peak of the triangle

carrier voltage waveform. When the sinusoidal waveform is greater than the triangular waveform, the upper switch is turned on and the lower switch is turned off. Similarly, when the sinusoidal waveform is less than the triangular waveform, the upper switch is off and the lower switch is on. Depending on the switching states, either the positive or negative half DC bus voltage is applied to each phase. The switches are controlled in pairs $((S_1, S_4), (S_3, S_6),$ and $(S_5, S_2))$ and the logic for the switch control signals is:

- S_1 is ON when $V_a > V_T$ S_4 is ON when $V_a < V_T$
- S_3 is ON when $V_b > V_T$ S_6 is ON when $V_b < V_T$
- S_5 is ON when $V_c > V_T$ S_2 is ON when $V_c < V_T$.
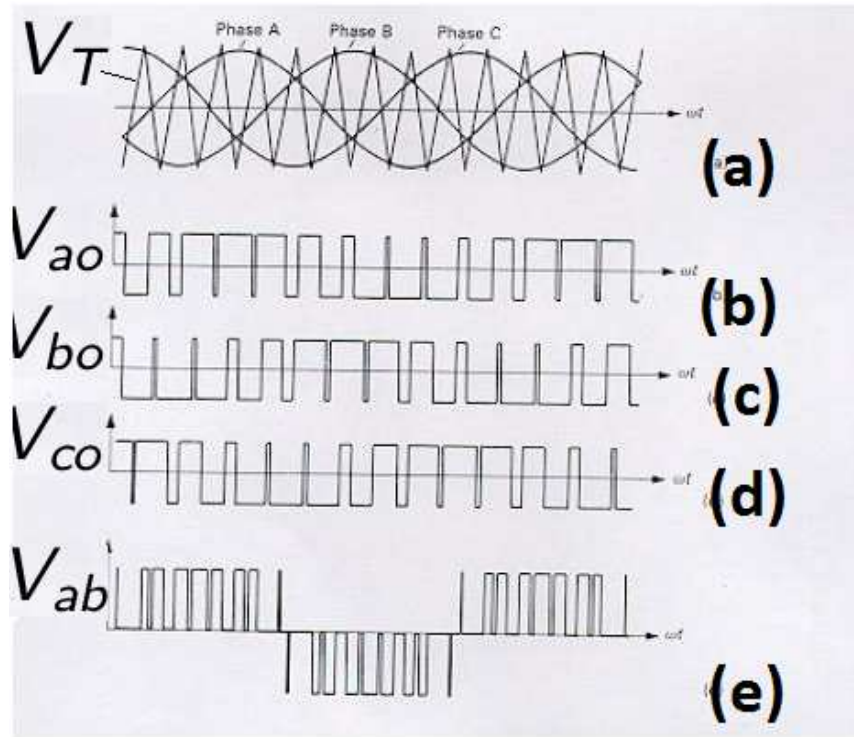
Figure 2.3: Three-Phase Sinusoidal PWM: a). Reference Voltages (a,b,c) and Triangular Wave b). V_{ao}, c) V_{bo}, d) V_{co} e) Line-to-Line Voltages [27].

As seen in Figure 2.3, the pulse widths depend on the intersection of the triangular and sinusoidal waveforms. The inverter output voltages are determined as follows:

$$
\begin{aligned}
\text{if} \quad && V_a > V_T \quad && \text{then} \quad && V_{ao} &= 0.5 V_{dc} \\
&& V_b > V_T \quad && \text{then} \quad && V_{bo} &= 0.5 V_{dc} \\
&& V_c > V_T \quad && \text{then} \quad && V_{co} &= 0.5 V_{dc} \\
\text{and if} \quad && V_a < V_T \quad && \text{then} \quad && V_{ao} &= -0.5 V_{dc} \\
&& V_b < V_T \quad && \text{then} \quad && V_{bo} &= -0.5 V_{dc} \\
&& V_c < V_T \quad && \text{then} \quad && V_{co} &= -0.5 V_{dc}.
\end{aligned}
$$

The inverter line-to-line voltages are obtained from the pole voltages as:

$$
\begin{aligned}
V_{ab} &= V_{ao} - V_{bo} \\
V_{bc} &= V_{bo} - V_{co} \\
V_{ca} &= V_{co} - V_{ao}.
\end{aligned}
$$

2.1.2 Modulation Index of Sinusoidal PWM

The Fourier series expansion of a symmetrical square wave voltage with a peak magnitude of $V_{dc}/2$ has a fundamental of magnitude $2V_{dc}/\pi$. The maximum of the output voltage generated by the SPWM method is $V_{dc}/2$. The modulation index is defined as the ratio of the magnitude of output voltage generated by SPWM to the fundamental peak value of the maximum square wave. Thus, the maximum modulation index of the SPWM technique is

$$
MI = \frac{V_{PWM}}{V_{max-sixstep}} = \frac{\frac{V_{dc}}{2}}{\frac{2V_{dc}}{\pi}} = \frac{\pi}{4} \approx 0.7855 = 78.55\%,
$$

where V_{PWM} is the maximum output voltage generated by a SPWM and $V_{max-sixstep}$ is the fundamental peak value of a square wave.

2.2 Third-Harmonic-Injection PWM

2.2.1 Concept and Calculation of Optimum Distortion

The sinusoidal PWM is the simplest modulation scheme to understand but it is unable to fully utilize the available DC bus supply voltage. Due to this problem, the third-harmonic-injection pulse-width modulation (THIPWM) technique was developed to improve the inverter performance.

Following Reference [17], consider a waveform consisting of a fundamental component with the addition of a triple-frequency term:

$$y = \sin\theta + A\sin 3\theta, \tag{2.1}$$

where $\theta = \omega t$ and A is a parameter to be optimized while keeping the maximum amplitude of $y(t)$ under unity. The maximum value of $y(t)$ is found by setting its derivative with respect to θ equal to zero. Thus,

$$\frac{dy}{d\theta} = \cos\theta + 3A\cos 3\theta = \cos\theta(12A\cos^2\theta - (9A - 1)) = 0. \tag{2.2}$$

The maximum and minimum of the waveform therefore occur at

$$\cos\theta = 0 \tag{2.3}$$

and

$$\cos\theta = \left(\frac{9A-1}{12A}\right)^{\frac{1}{2}} \tag{2.4}$$

which yield, respectively,

$$\sin\theta = 1 \tag{2.5}$$

and

$$\sin\theta = \left(\frac{1+3A}{12A}\right)^{\frac{1}{2}}. \tag{2.6}$$

The peak value of y can be found by substituting the values obtained for $\sin\theta$ in (2.5) and (2.6) into (2.1). Using the following trigonometric identity,

$$\sin 3\theta = 3\sin\theta - 4\sin^3\theta, \tag{2.7}$$

Equation (2.1) becomes

$$y = (1+3A)\sin\theta - 4A\sin^3\theta. \tag{2.8}$$

Substituting the values in (2.5) and (2.6), for $\sin\theta$ we have

$$\widehat{y} = 1 - A \tag{2.9}$$

and

$$\widehat{y} = 8A\left(\frac{1+3A}{12A}\right)^{\frac{3}{2}}, \tag{2.10}$$

where $\widehat{y}$ is the peak value of y.

The optimum value for A is that value which minimizes $\widehat{y}$ and can be found by differentiating (2.10) for $\widehat{y}$ with respect to A and equating the result to zero. Then, Equation (2.10) becomes,

$$\frac{d\widehat{y}}{dA} = \left(\frac{1+3A}{12A}\right)^{\frac{1}{2}} \left(2 - \frac{1}{3A}\right) = 0. \tag{2.11}$$

Thus, the two possible values of A are

$$A = -\frac{1}{3} \quad \text{and} \quad A = \frac{1}{6}. \tag{2.12}$$

From Equation (2.9), we can see that the negative value of A makes $\widehat{y}$ greater than unity. Therefore, the only valid solution for A is 1/6 and the required waveform is

$$y = \sin\theta + \frac{1}{6}\sin 3\theta. \tag{2.13}$$

From Equation (2.3), $\cos\theta = 0$ yields $\theta = \pi/2$. Substituting the value of 1/6 for A in (2.4) gives $\cos\theta = 1/2$, i.e., $\theta = \pi/3, 2\pi/3$, etc. All triple harmonics pass through zero at these values of θ. If we substitute the values of $\theta = n\pi/3$ in (2.13), then we have a maximum amplitude of $\widehat{y} = \pm\sqrt{3}/2$ at these angles.

In Figure 2.4, it is shown that the addition of a third harmonic with a peak magnitude of one sixth to the modulation waveform has the effect of reducing the peak value of the output waveform by a factor of $\sqrt{3}/2$ without changing the amplitude of the fundamental. It is possible to increase the amplitude of the modulating waveform by a factor K, so that the full output voltage range of the inverter is again utilized [17]. If the modulating waveform is expressed as

$$y = K\left(\sin\theta + \frac{1}{6}\sin 3\theta\right), \tag{2.14}$$

the required factor K for a peak value of unity should satisfy the constraint

$$1 = K\sqrt{3}/2 \tag{2.15}$$

and, therefore,

$$K = \frac{2}{\sqrt{3}}. \tag{2.16}$$

On the same figure, we see that the addition of this third harmonic produces a 15.5% increase in the amplitude of the fundamental of the phase voltages. Figure 2.4(a) does not have a third harmonic, only a peak value and amplitude of fundamental equal 1. The peak of Figure 2.4(b) is $\sqrt{3}/2$ with one-sixth of the third harmonic added. The amplitude of the fundamental equals 1. The peak amplitude in Figure 2.4(c) equals 1 while the peak amplitude of the fundamental equals $2/\sqrt{3}$ with one-sixth of third harmonic added. Injecting a third harmonic component to the fundamental component gives the following modulating waveforms for the three-phase [17]:

$$V_{an} = \frac{2}{\sqrt{3}}\left(\sin(\omega t) + \frac{1}{6}\sin(3\omega t)\right) \tag{2.17}$$

$$V_{bn} = \frac{2}{\sqrt{3}}\left(\sin(\omega t - 2\pi/3) + \frac{1}{6}\sin(3\omega t)\right) \tag{2.18}$$

$$V_{cn} = \frac{2}{\sqrt{3}}\left(\sin(\omega t + 2\pi/3) + \frac{1}{6}\sin(3\omega t)\right). \tag{2.19}$$

The THIPWM is implemented in the same manner as the SPWM, that is, the reference waveforms are compared with a triangular waveform. As a result, the amplitude of the reference waveforms do not exceed the DC supply voltage $V_{dc}/2$, but the fundamental component is higher than the supply voltage V_{dc}. As mentioned above, this is approximately 15.5% higher in amplitude than the normal sinusoidal PWM. Consequently, it
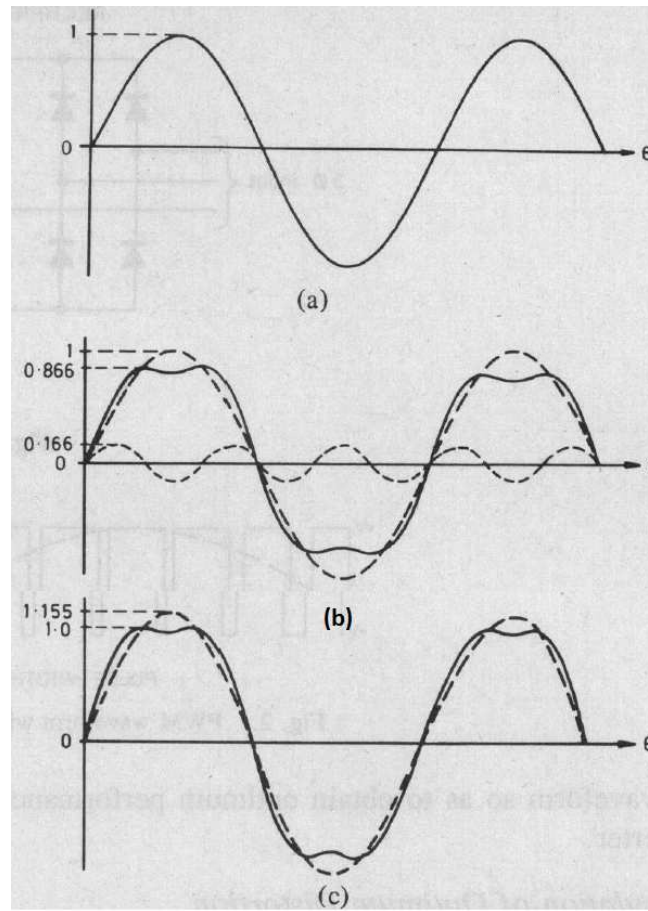
Figure 2.4: One-Phase Third-Harmonic Injection PWM [17].

provides a better utilization of the DC supply voltage.

The three reference voltages and triangular waveform of a three-phase THPWM produce the following output pole voltages V_{ao}, V_{bo}, V_{co} shown in Figure 2.5.
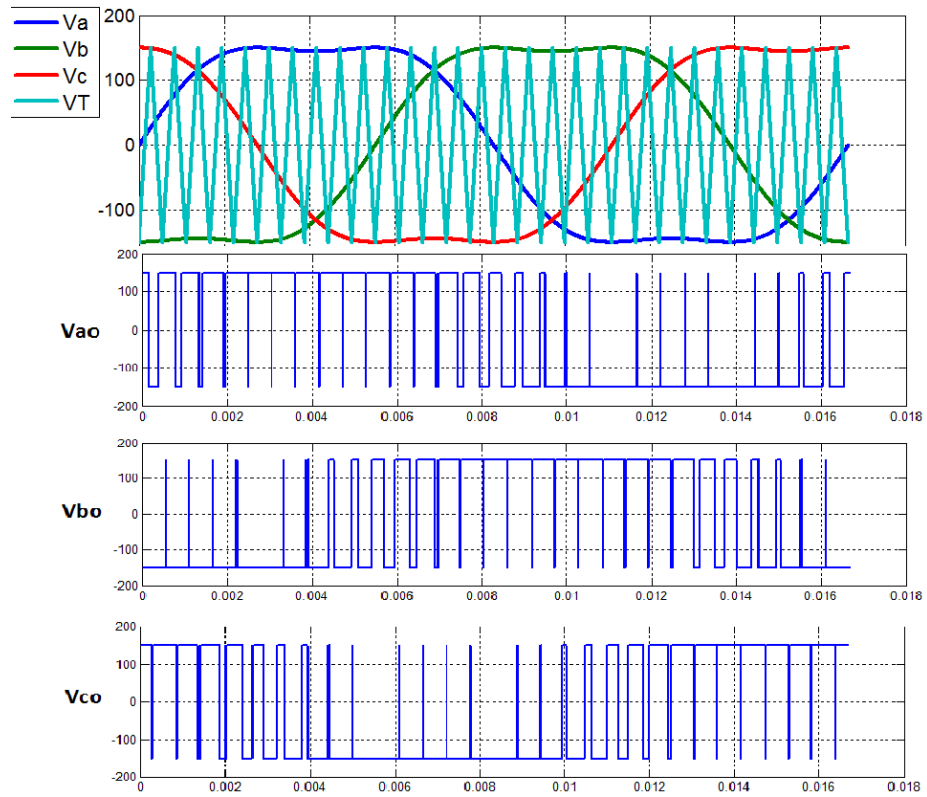
Figure 2.5: Reference Voltages (a,b,c), Triangular Waveforms (V_T), and Output Voltage (V_{ao}, V_{bo}, V_{co}).

CHAPTER 3

SPACE VECTOR PWM

3.1 Introduction

Another method for increasing the output voltage about that of the SPWM technique is the space vector PWM (SVPWM) technique. Compared to THIPWM, the two methods have similar results but their methods of implementation are completely different. In the SVPWM technique, the duty cycles are computed rather than derived through comparison as in SPWM. The SVPWM technique can increase the fundamental component by up to 27.39% that of SPWM. The fundamental voltage can be increased up to a square wave mode where a modulation index of unity is reached.

SVPWM is accomplished by rotating a reference vector around the state diagram, which is composed of six basic non-zero vectors forming a hexagon. A circle can be inscribed inside the state map and corresponds to sinusoidal operation. The area inside the inscribed circle is called the linear modulation region or under-modulation region. As seen in Figure 3.1, the area between the inside circle and outside circle of the hexagon is called the nonlinear modulation region or over-modulation region. The concepts in the operation of linear and nonlinear modulation regions depend on the modulation index, which indirectly reflects on the inverter utilization capability.
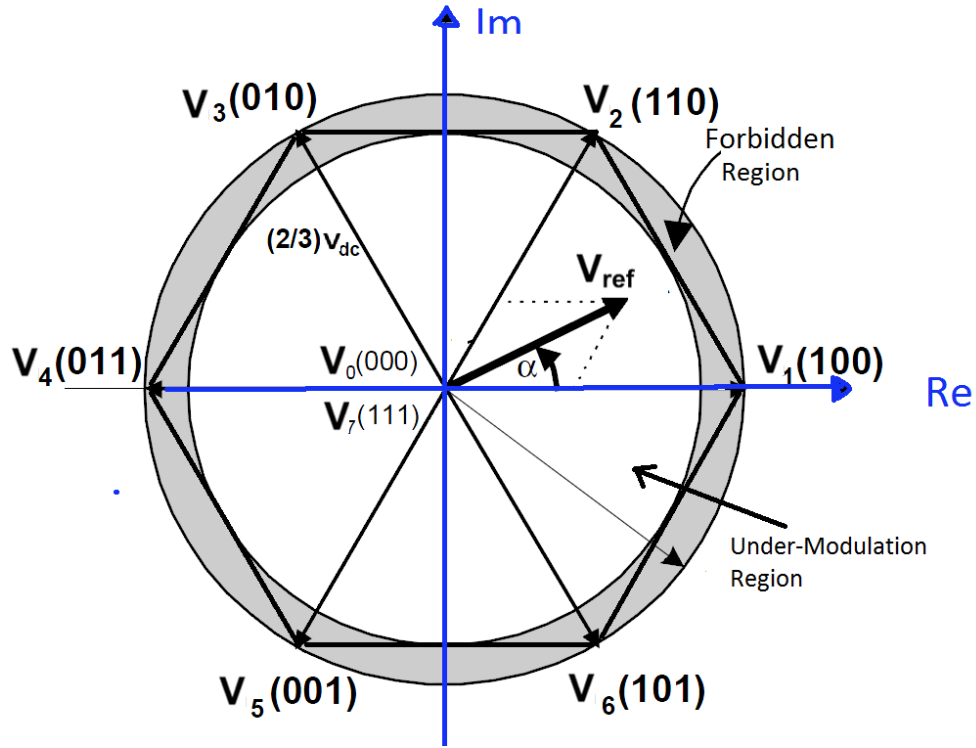
Figure 3.1: Under-modulation and Over-modulation Regions in Space Vector Representation [12].

3.2 Principle of Space Vector PWM

A three-phase mathematical system can be represented by a space vector. For example, given a set of three-phase voltages, a space vector can be defined by

$$\overrightarrow{V}(t) = \frac{2}{3}[V_a(t)e^{j0} + V_b(t)e^{j\frac{2\pi}{3}} + V_c(t)e^{j\frac{4\pi}{3}}], \tag{3.1}$$

where V_a(t), V_b(t), and V_c(t) are three sinusoidal voltages of the same amplitude and frequency but with $\pm 120^o$ phase shifts. The space vector at any given time maintains its magnitude. As time increases, the angle of the space vector increases, causing the vector to rotate with a frequency equal to that of the sinusoidal waveforms. When the output

voltages of a three-phase six-step inverter are converted to a space vector and plotted on the complex plane, the corresponding space vector takes only on one of six discrete angles as time increases. The central idea of SVWPM is to generate appropriate PWM signals so that a vector with any desired angle can be generated.

SVPWM is a form of PWM proposed in the mid-1980s that is more efficient compared to natural and regularly-sampled PWM. In the space-vector modulation, a three-phase two-level inverter can be driven to eight switching states where the inverter has six active states (1-6) and two zero states (0 and 7).

A typical two-level inverter has 6 power switches (labeled S_1 to S_6) that generate three-phase voltage outputs. A detailed drawing of a three-phase bridge inverter is shown in Figure 3.2. The circuit has a full-bridge topology with three inverter legs, each consisting of two power switches. The circuit allows only positive power flow from the supply system to the load via a full-bridge diode rectifier. Negative power flow is not possible through the rectifier diode bridge.

The six switching power devices can be constructed using power BJTs, GTOs, IGBTs, etc. The choice of switching devices is based on the desired operating power level, required switching frequency, and acceptable inverter power losses. When an upper transistor is switched on, the corresponding lower transistor is switched off. Therefore, the ON and OFF states of the upper transistors S_1, S_3, S_5 can be used to determine the current output voltage. The ON and OFF states of the lower power devices are complementary to the upper ones. Two switches on the same leg cannot be closed or opened at the same time.

The basic principle of SVPWM is based on the eight switch combinations of a three-phase inverter. The switch combinations can be represented as binary codes that correspond to the top switches S_1, S_3, and S_5 of the inverter as shown in Figure 3.2. Each switching circuit generates three independent pole voltages V_{ao}, V_{bo}, and V_{co}, which are
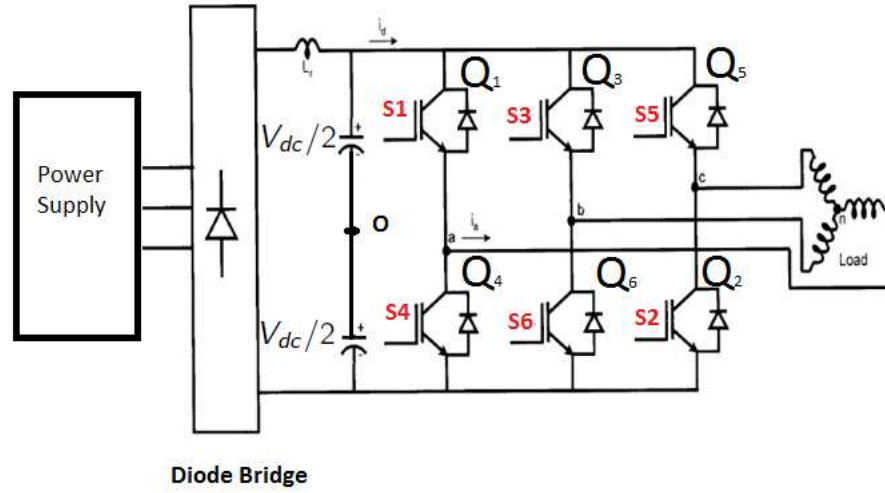
Figure 3.2: Three-Phase Bridge Inverter [11].

the inverter output voltages with respect to the mid-terminal of the DC source marked as 'O' on the same figure. These voltages are also called pole voltages.

The pole voltages that can be produced are either $V_{dc}/2$ or $-V_{dc}/2$. For example, when switches S_1, S_6, and S_2 are closed, the corresponding pole voltages are $V_{ao} = V_{dc}/2$, $V_{bo} = -V_{dc}/2$, and $V_{co} = -V_{dc}/2$. This state is denoted as (1,0,0) and, according to Equation (3.1), may be depicted as the space vector $\overrightarrow{V}(t) = \frac{2}{3}[V_{dc}e^{j0}]$. Repeating the same procedure, we can find the remaining active and non-active states shown in Figure 3.3.

The three-phase inverter is therefore controlled by six switches and eight inverter configurations. The eight inverter states can be transformed into eight corresponding space vectors. In each configuration, the vector identification uses a '0' to represent the negative phase voltage level and a '1' to represent the positive phase voltage level. The relationship between the space vector and the corresponding switching states is given in Table 3.1 and Figure 3.2. In addition, the switches in one inverter branch are in controlled in a complementary fashion (1 if the switch is on and 0 if it is off). Therefore,
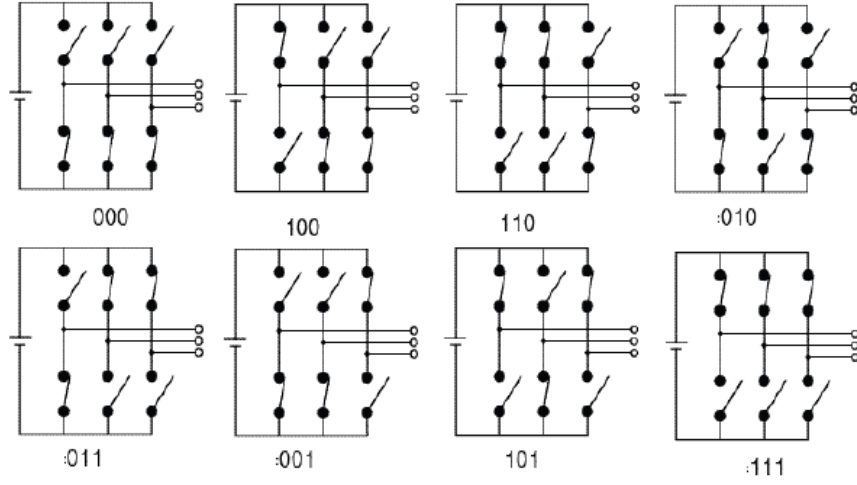
Figure 3.3: Eight Switching Configuration of a Three-Phase Inverter [7].

$$S1 + S4 = 1;$$

$$S2 + S6 = 1;$$

$$S5 + S2 = 1.$$

We use orthogonal coordinates to represent the three-phase two-level inverter in the phase diagram. There are eight possible inverter states that can generate eight space vectors. These are given by the complex vector expressions:

$$\overrightarrow{V}_k = \begin{cases} \frac{2}{3} V_{dc} e^{j(k-1)\frac{\pi}{3}} & \text{if } k = 1,2,3,4,5,6 \\ 0 & \text{if } k = 0,7. \end{cases} \tag{3.2}$$

The entire space is divided into six equal-size sectors of 60°. Each sector is bounded by two active vectors. $\overrightarrow{V}_0$ and $\overrightarrow{V}_7$ are two voltage vectors with zero amplitude located at the origin of the hexagon. The eight active and non-active state vectors are geometrically drawn in Figure 3.4.

Table 3.1: Space Vectors, Switching States, and On State Switches

Space Vetor	Swtiching State	On-state Switch	Vector Definition
$\vec{V}_0$	[000]	S4,S6,S2	$\vec{V}_0 = 0$
$\vec{V}_1$	[100]	S1,S6,S2	$\vec{V}_1 = \frac{2}{3}V_{dc}e^{j0}$
$\vec{V}_2$	[110]	S1,S3,S2	$\vec{V}_2 = \frac{2}{3}V_{dc}e^{j\frac{\pi}{3}}$
$\vec{V}_3$	[010]	S4,S3,S2	$\vec{V}_3 = \frac{2}{3}V_{dc}e^{j\frac{2\pi}{3}}$
$\vec{V}_4$	[011]	S4,S3,S5	$\vec{V}_4 = \frac{2}{3}V_{dc}e^{j\frac{3\pi}{3}}$
$\vec{V}_5$	[001]	S4,S6,S5	$\vec{V}_5 = \frac{2}{3}V_{dc}e^{j\frac{4\pi}{3}}$
$\vec{V}_6$	[101]	S1,S6,S5	$\vec{V}_6 = \frac{2}{3}V_{dc}e^{j\frac{5\pi}{3}}$
$\vec{V}_7$	[111]	S1,S3,S5	$\vec{V}_7 = \frac{2}{3}V_{dc}e^{j0}$

The reference voltage vector $\vec{V}_{ref}$ rotates in space at an angular velocity $\omega = 2\pi f$, where f is the fundamental frequency of the inverter output voltage. When the reference voltage vector passes through each sector, different sets of switches in Table 3.1 will be turned on or off. As a result, when the reference voltage vector rotates through one revolution in space, the inverter output varies one electrical cycle over time. The inverter output frequency coincides with the rotating speed of the reference voltage vector. The zero vectors ($\vec{V}_0$ and $\vec{V}_7$) and active vectors ($\vec{V}_1$ to $\vec{V}_6$) do not move in space. They are referred to as stationary vectors. Figure 3.4 shows the reference vector $\vec{V}_{ref}$ in the first sector.

The six active voltage space vectors are shown on the same graph with an equal magnitude of $2V_{dc}/3$ and a phase displacement of 60°. The inverter cannot produce a desired reference voltage vector directly. It is possible to decompose the reference vector into vectors that lie on two adjacent active vectors and two zero vectors, which are located at the center of the hexagon.

The relationship between the switching variable vector $[S_1, S_3, S_5]$ and the line-to-line
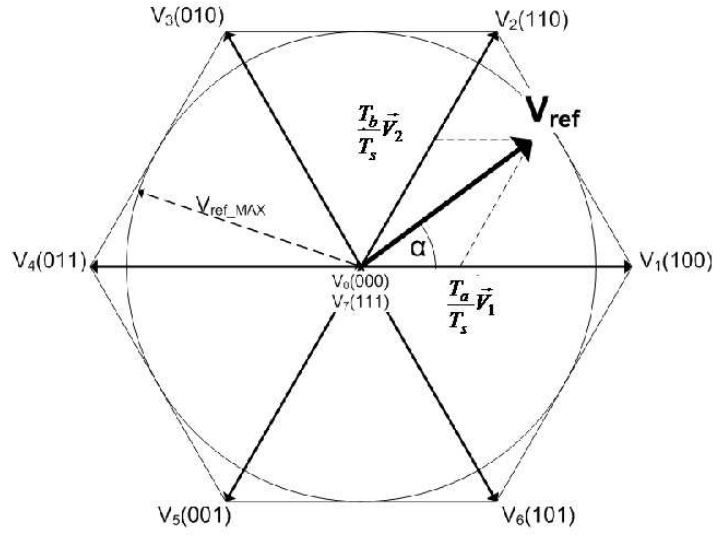
Figure 3.4: Space Vectors of Three-Phase Bridge Inverter [12].

voltage vector $[V_{ab}, V_{bc}, V_{ca}]$ is shown in Equation (3.1). When the upper or lower transistor of a phase is ON, the switching signal of that phase is '1' or '-1', and when an upper or lower transistor is OFF, then the switching signal is '0'. The eight combinations and the derived output line-to-line and phase voltages in terms of the DC supply voltage are:

$$
\begin{bmatrix} V_{ab} \\ V_{bc} \\ V_{ca} \end{bmatrix} = V_{dc} \begin{bmatrix} 1 & -1 & 0 \\ 0 & 1 & -1 \\ -1 & 0 & 1 \end{bmatrix} \begin{bmatrix} S_1 \\ S_3 \\ S_5 \end{bmatrix}.
\tag{3.3}
$$

Choosing a neutral load point n, we have:

$$
\begin{cases}
V_{a0} &= V_{an} + V_{n0} \\
V_{b0} &= V_{bn} + V_{n0} \\
V_{c0} &= V_{cn} + V_{n0} \\
V_{an} + V_{bn} + V_{cn} &= 0.
\end{cases}
\tag{3.4}
$$

From Equations (3.3) and (3.4), the output phase voltages of the inverter depend on the relationship between the switching variables $[S_1, S_3, S_5]$ and the DC voltage as follows:

$$
\begin{bmatrix} V_{an} \\ V_{bn} \\ V_{cn} \end{bmatrix} = \frac{V_{dc}}{3} \begin{bmatrix} 2 & -1 & -1 \\ -1 & 2 & -1 \\ -1 & -1 & 2 \end{bmatrix} \begin{bmatrix} S_1 \\ S_3 \\ S_5 \end{bmatrix}.
\tag{3.5}
$$

According to the Equations (3.3) to (3.5), the eight switching vectors, output line-to-neutral voltage (phase voltages), and output line-to-line voltages in terms of DC link V_{dc} are given in Table 3.2 along with the eight inverter voltage vectors ($\overrightarrow{V}_0$ to $\overrightarrow{V}_7$).

Table 3.2: Vectors, Switching Vectors, Phase Voltages and Line to Line Voltages as a Function of the DC Bus Voltage V_{dc}.

Voltage Vectors	Switching Vectors			Line-to-Neutral Voltages			Line-to-Line Voltages		
	a	b	c	V_{an}	V_{bn}	V_{cn}	V_{ab}	V_{bc}	V_{ca}
V_0	0	0	0	0	0	0	0	0	0
V_1	1	0	0	$\frac{2V_{dc}}{3}$	$-\frac{V_{dc}}{3}$	$-\frac{V_{dc}}{3}$	V_{dc}	0	$-V_{dc}$
V_2	1	1	0	$\frac{V_{dc}}{3}$	$\frac{V_{dc}}{3}$	$-\frac{2V_{dc}}{3}$	0	V_{dc}	$-V_{dc}$
V_3	0	1	0	$-\frac{V_{dc}}{3}$	$\frac{2V_{dc}}{3}$	$-\frac{V_{dc}}{3}$	$-V_{dc}$	V_{dc}	0
V_4	0	1	1	$-\frac{2V_{dc}}{3}$	$\frac{V_{dc}}{3}$	$\frac{V_{dc}}{3}$	$-V_{dc}$	0	V_{dc}
V_5	0	0	1	$-\frac{V_{dc}}{3}$	$-\frac{V_{dc}}{3}$	$\frac{2V_{dc}}{3}$	0	$-V_{dc}$	V_{dc}
V_6	1	0	1	$\frac{V_{dc}}{3}$	$-\frac{2V_{dc}}{3}$	$\frac{V_{dc}}{3}$	V_{dc}	$-V_{dc}$	0
V_7	1	1	1	0	0	0	0	0	0

The space vector can be also represented in another reference frame with two orthogonal axes (α and β). We assume that the α axis is aligned in the horizontal direction and that the β axis is vertical. Then the abc three-phase voltage vector given in Equation (3.1) can be transformed into a vector with $\alpha\beta$ coordinates. The $\alpha\beta$ vector is used to find

the sector of the $\alpha\beta$ plane in which the reference voltage vector lies. The phase voltages corresponding to the eight combinations of switching patterns can be mapped into $\alpha\beta$ coordinates:

$$\overrightarrow{V}_{ref} = V_\alpha + jV_\beta = \frac{2}{3}(V_a + V_b e^{j\frac{2\pi}{3}} + V_c e^{-j\frac{2\pi}{3}}) \tag{3.6}$$

$$V_\alpha + jV_\beta = \frac{2}{3}(V_a + V_b\cos(\frac{2\pi}{3}) + V_c\cos(\frac{2\pi}{3})) + j\frac{2}{3}(V_b\sin(\frac{2\pi}{3}) - V_c\cos(\frac{2\pi}{3})).$$

Equating real and imaginary parts, we get

$$V_\alpha = \frac{2}{3}(V_a + V_b\cos(\frac{2\pi}{3}) + V_c\cos(\frac{2\pi}{3})) \tag{3.7}$$

$$V_\beta = \frac{2}{3}(V_b\sin(\frac{2\pi}{3}) - V_c\cos(\frac{2\pi}{3})). \tag{3.8}$$

In matrix form, these equations become:

$$\overrightarrow{V}_{ref} = \begin{bmatrix} V_\alpha \\ V_\beta \end{bmatrix} = \frac{2}{3}\begin{bmatrix} 1 & -1/2 & -1/2 \\ 0 & \sqrt{3}/2 & -\sqrt{3}/2 \end{bmatrix}\begin{bmatrix} V_a \\ V_b \\ V_c \end{bmatrix}. \tag{3.9}$$

The values of V_α and V_β in Table 3.3 are called the α and β components of the space vector, and the last column in Table 3.3 shows the reference space vector. The voltages V_α and V_β become the inputs for dwelling time calculations in the space vector PWM and are used to compute the scalar magnitude of the reference voltage $|\overrightarrow{V}_{Ref}|$.

3.3   Implementation Procedure of a Two-Level Space Vector PWM

The SVPWM scheme is more complicated than that of the conventional SPWM. It requires the determination of a sector, calculation of vector segments, and it involves region identification based on the modulation index and calculation of switching time durations.

Table 3.3: Voltage Vectors, Switching Vector, α and β

Voltage Vector	a	b	c	V_α	V_β	Vector
V_0	0	0	0	0	0	0
V_1	1	0	0	$\frac{2V_{dc}}{3}$	0	V_{0^o}
V_2	1	1	0	$\frac{V_{dc}}{3}$	$\frac{V_{dc}}{\sqrt{3}}$	V_{60^o}
V_3	0	1	0	$-\frac{V_{dc}}{3}$	$\frac{V_{dc}}{\sqrt{3}}$	V_{120^o}
V_4	0	1	1	$\frac{2V_{dc}}{3}$	0	V_{180^o}
V_5	0	0	1	$-\frac{V_{dc}}{3}$	$-\frac{V_{dc}}{\sqrt{3}}$	V_{240^o}
V_6	1	0	1	$\frac{V_{dc}}{3}$	$-\frac{V_{dc}}{\sqrt{3}}$	V_{300^o}
V_7	1	1	1	0	0	0
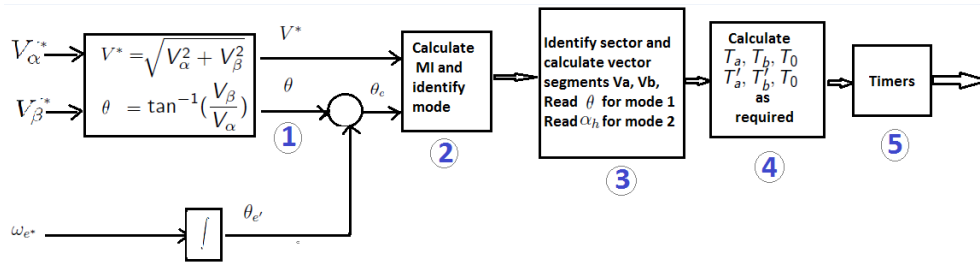
Figure 3.5: Flow Diagram for SVPWM Implementation [11].

A simplified flow diagram for the implementation of the SVPWM algorithm is shown in Figure 3.5. The procedure for implementing a two-level space vector PWM can be summarized as follows:

1. Calculate the angle θ and reference voltage vector $\overrightarrow{V}_{ref}$ based on the input voltage components.

2. Calculate the modulation index and determine if it is in the over-modulation region.

3. Find the sector in which $\overrightarrow{V}_{ref}$ lies, and the adjacent space vectors of $\overrightarrow{V}_k$ and $\overrightarrow{V}_{k+1}$

based on the sector angle θ.

4. Find the time intervals T_a and T_b and T_0 based on T_s, and the angle θ. (For over-modulation, find T_a', T_b' and T_0' is zero.)

5. Determine the modulation times for the different switching states.

3.3.1 Angle and Reference Voltage Vector

In the Space Vector PWM, the three-phase output voltage vector is represented by a reference vector that rotates at an angular speed of $\omega = 2\pi f$. The Space Vector PWM uses the combinations of switching states to approximate the reference vector $\overrightarrow{V}_{ref}$. A reference voltage vector $\overrightarrow{V}_{ref}$ that rotates with angular speed ω in the $\alpha\beta$ plane represents three sinusoidal waveforms with angular frequency ω in the abc coordinate system. Each output voltage combination in Table 3.3 corresponds to a different voltage space vector. Three sinusoidal and balanced voltages are given by the relations:

$$V_a(t) \;=\; V_{ref}\cos(\omega t) \tag{3.10}$$

$$V_b(t) \;=\; V_{ref}\cos(\omega t - 2\pi/3) \tag{3.11}$$

$$V_c(t) \;=\; V_{ref}\cos(\omega t + 2\pi/3). \tag{3.12}$$

For any three-phase system with three wires and equal load impedances, we have

$$V_a(t) + V_b(t) + V_c(t) = 0. \tag{3.13}$$

The space vector with magnitude V_{ref} rotates in a circular direction at an angular velocity of ω where the direction of rotation depends on the phase sequence of the voltages. If it has a positive phase sequence, then it rotates in the counterclockwise direction. Otherwise, it rotates in the clockwise direction with a negative phase sequence.

The three-phase voltages could be described with only two components, α and β, in a two-dimensional plane. The magnitude of each active vector is $2V_{dc}/3$. The active vectors are 60° apart and describe a hexagon boundary. The locus of the circle projected by the space reference vector $\overrightarrow{V}_{ref}$ depends on $\overrightarrow{V}_0, \overrightarrow{V}_1, \overrightarrow{V}_2, \overrightarrow{V}_3, \overrightarrow{V}_4, \overrightarrow{V}_5, \overrightarrow{V}_6, \overrightarrow{V}_7$,

$$\overrightarrow{V}_{ref} = \frac{2}{3}[V_a + aV_b + a^2V_c] \tag{3.14}$$

where $a = e^{j2\pi/3}$. The magnitude of the reference vector is:

$$|\overrightarrow{V}_{ref}| = \sqrt{V_\alpha^2 + V_\beta^2}. \tag{3.15}$$

The phase angle is evaluated from

$$\theta = \tan^{-1}(\frac{V_\beta}{V_\alpha}), \tag{3.16}$$

where $\theta \in [0, 2\pi]$.

3.3.2 Modulation Index of Linear Modulation

In the linear region, the rotating reference vector always remains within the hexagon. The largest output voltage magnitude is the radius of the largest circle that can be inscribed within the hexagon. This means that the linear region ends when the reference voltage is equal to the radius of the circle inscribed within the hexagon.

The fundamental component of the voltage waveform is shown in Figure 3.6. From a Fourier analysis, the fundamental voltage magnitude is given by

$$
\begin{aligned}
V_{max-sixstep} &= \frac{4}{\pi}\left[\int_0^{\pi/3}\frac{V_{dc}}{3}\sin\theta\,d\theta + \int_{\pi/3}^{\pi/2}\frac{2V_{dc}}{3}\sin\theta\,d\theta\right]\\
&= \frac{4V_{dc}}{3\pi}\left[\left(-\cos\frac{\pi}{3}+1\right)+\left(-2\cos\frac{\pi}{2}+2\cos\frac{\pi}{3}\right)\right]\\
&= \frac{4V_{dc}}{3\pi}\left[1+\cos\frac{\pi}{3}\right]\\
&= \frac{2V_{dc}}{\pi}.
\end{aligned}
\tag{3.17}
$$

The ratio between the reference vector $\overrightarrow{V}_{ref}$ and the fundamental peak value of the square
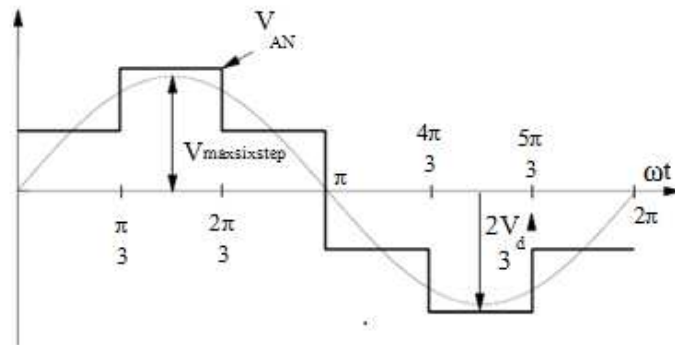
Figure 3.6: Fundamental of Voltage Waveform [10].

phase voltage wave $(2V_{dc}/\pi)$ is called the modulation index. The mode of operation is determined by the modulation index (MI). In this linear region, the MI can be expressed as:

$$
MI = \frac{\overrightarrow{V}_{ref}}{V_{max-sixstep}}.
\tag{3.18}
$$

From the geometry of Figure 3.1, the maximum modulation index is obtained when $\overrightarrow{V}_{ref}$ equals the radius of the inscribed circle.

$$
\overrightarrow{V}_{ref(max)} = \frac{2}{3}V_{dc}\cos(\pi/6).
\tag{3.19}
$$

Therefore,

$$MI_{max} = \frac{\frac{2}{3}V_{dc}\cos(\frac{\pi}{6})}{\frac{2V_{dc}}{\pi}} = 0.907. \tag{3.20}$$

3.3.3 Sector Determination

It is necessary to know in which sector the reference output lies in order to determine the switching time and sequence. The identification of the sector where the reference vector is located is straightforward. The phase voltages correspond to eight switching states: six non-zero vectors and two zero vectors at the origin. Depending on the reference voltages V_α and V_β, the angle of the reference vector can be used to determine the sector as per Table 3.4.

Table 3.4: Sector Definition.

Sector	Degrees
1	$0 < \theta \leq 60\,^o$
2	$60 < \theta \leq 120^o$
3	$120 < \theta \leq 180^o$
4	$180 < \theta \leq 240^o$
5	$240 < \theta \leq 300^o$
6	$300 < \theta \leq 360^o$

3.3.4 Time Durations T_a, T_b, T_0

The duty cycle computation is done for each triangular sector formed by two state vectors. The magnitude of each switching state vector is $2V_{dc}/3$ and the magnitude of a vector to the midpoint of the hexagon line from one vertex to another is $V_{dc}/\sqrt{3}$. In the under-modulation, the maximum possible modulation index is 0.907 as derived previously.

The reference space vector rotates and moves through different sectors of the complex plane as time increases. In each PWM cycle, the reference vector $\overrightarrow{V}_{ref}$ is sampled at a fixed input sampling frequency f_s. During this time, the sector is determined and the modulation vector $\overrightarrow{V}_{ref}$ is mapped onto two adjacent vectors. The non-zero vectors can be represented by

$$\overrightarrow{V}_k = \frac{2}{3}V_{dc}e^{j(k-1)\frac{\pi}{3}} \tag{3.21}$$

for k=1, 2, 3, 4, 5, 6.

Therefore, the non-zero vectors for $\overrightarrow{V}_k$ and $\overrightarrow{V}_{k+1}$ become

$$\overrightarrow{V}_k = \frac{2}{3}V_{dc}[\cos(k-1)\frac{\pi}{3} + j\sin(k-1)\frac{\pi}{3}]$$
$$\overrightarrow{V}_{k+1} = \frac{2}{3}V_{dc}e^{jk\frac{\pi}{3}} = \frac{2}{3}V_{dc}[\cos\frac{k\pi}{3} + j\sin\frac{k\pi}{3}].$$

Due to symmetry in the patterns in the six sectors, the integration

$$\int_0^{\frac{T_s}{2}} \overrightarrow{V}_{ref}\,dt = \int_0^{\frac{T_0}{4}} \overrightarrow{V}_0\,dt + \int_{\frac{T_0}{4}}^{\frac{T_0}{4}+T_a} \overrightarrow{V}_k\,dt + \int_{\frac{T_0}{4}+T_a}^{\frac{T_0}{4}+T_a+T_b} \overrightarrow{V}_{k+1}\,dt + \int_{\frac{T_0}{4}+T_a+T_b}^{\frac{T_s}{2}} \overrightarrow{V}_7\,dt \tag{3.22}$$

can be carried out for only half of the pulse-width modulation period $(T_s/2)$. Zero voltages are applied during the null state times:

$$\int_0^{\frac{T_0}{4}} \overrightarrow{V}_0\,dt = \int_{\frac{T_0}{4}+T_a+T_b}^{\frac{T_s}{2}} \overrightarrow{V}_7\,dt = 0. \tag{3.23}$$

Then Equation (3.22) becomes:

$$\int_0^{\frac{T_s}{2}} \overrightarrow{V}_{ref}\,dt = \int_{\frac{T_0}{4}}^{\frac{T_0}{4}+T_a} \overrightarrow{V}_k\,dt + \int_{\frac{T_0}{4}+T_a}^{\frac{T_0}{4}+T_a+T_b} \overrightarrow{V}_{k+1}\,dt. \tag{3.24}$$

Thus, the product of the reference voltage vector $\overrightarrow{V}_{ref}$ and $T_s/2$ equals the sum of the

voltage multiplied by the time interval of the chosen space vectors. The reference voltage vector $\overrightarrow{V}_{ref}$ can be expressed as function of V_k and V_{k+1} as

$$\overrightarrow{V}_{ref}\frac{T_s}{2} = \overrightarrow{V}_k T_a + \overrightarrow{V}_{k+1} T_b$$

$$\overrightarrow{V}_{ref} = V_\alpha + jV_\beta,$$

(3.25)

where T_a and T_b denote the required on-time of the active-state vectors $\overrightarrow{V}_k$ and $\overrightarrow{V}_{k+1}$ during each sample period, and k is the sector number denoting the reference location. The calculated times T_a and T_b are applied to the switches to produce space vector PWM switching patterns based on each sector. The switching time is arranged according to the first half of the switching period while the other half is a reflection forming a symmetrical pattern (see Figure 3.7). T_0 and T_7 are the times of the null state vectors in Figure 3.7.

If $\overrightarrow{V}_{ref}$ lies exactly in the middle between two vectors, for example between $\overrightarrow{V}_1$ and $\overrightarrow{V}_2$ with an angle of $\pi/6$, T_a for $\overrightarrow{V}_1$ will be equal to T_b for $\overrightarrow{V}_2$. If $\overrightarrow{V}_{ref}$ is closer to $\overrightarrow{V}_2$ than $\overrightarrow{V}_1$, it means that T_b will be greater than T_a. If $\overrightarrow{V}_{ref}$ coincides with $\overrightarrow{V}_2$, then T_a will be equal to zero. If the reference keeps making a circular trajectory inside the hexagon, then T_0 is greater than zero, the output voltage will be a sinusoidal waveform in the under-modulation region.

Assuming that the reference voltage and the voltage vectors $\overrightarrow{V}_k$ and $\overrightarrow{V}_{k+1}$ are constant during each pulse-width modulation period T_s and splitting the reference voltage $\overrightarrow{V}_{ref}$ into its real and imaginary components (V_α and V_β) gives the following result:

$$\begin{bmatrix} V_\alpha \\ V_\beta \end{bmatrix} \frac{T_s}{2} = \frac{2V_{dc}}{3} \left(T_a \begin{bmatrix} \cos\frac{(k-1)\pi}{3} \\ \sin\frac{(k-1)\pi}{3} \end{bmatrix} + T_b \begin{bmatrix} \cos\frac{k\pi}{3} \\ \sin\frac{k\pi}{3} \end{bmatrix} \right)$$

or

$$= \frac{2}{3} V_{dc} \begin{bmatrix} \cos \frac{(k-1)\pi}{3} & \cos \frac{k\pi}{3} \\ \sin \frac{(k-1)\pi}{3} & \sin \frac{k\pi}{3} \end{bmatrix} \begin{bmatrix} T_a \\ T_b \end{bmatrix}. \tag{3.26}$$

These equations require computations involving trigonometric functions. From the Equation (3.26), the inverse matrix is used to calculate T_a and T_b as:

$$\begin{bmatrix} T_a \\ T_b \end{bmatrix} = \frac{\sqrt{3} T_s}{2 V_{dc}} \begin{bmatrix} \sin \frac{k\pi}{3} & -\cos \frac{k\pi}{3} \\ -\sin \frac{(k-1)\pi}{3} & \cos \frac{(k-1)\pi}{3} \end{bmatrix} \begin{bmatrix} V_\alpha \\ V_\beta \end{bmatrix}. \tag{3.27}$$

The Space Vector PWM produces the following balanced set of three-phase voltages with magnitude $\vec{V}_{ref}$ and angular frequency ω, given by:

$$V_a = V_{ref} \cos(\omega t) \tag{3.28}$$

$$V_b = V_{ref} \cos(\omega t - \frac{2\pi}{3}) \tag{3.29}$$

$$V_c = V_{ref} \cos(\omega t - \frac{4\pi}{3}). \tag{3.30}$$

The corresponding reference voltage space vector can be expressed as

$$\vec{V}_{ref} = |\vec{V}_{ref}| e^{j\omega t} = |\vec{V}_{ref}|(\cos \omega t + j \sin \omega t). \tag{3.31}$$

Equation (3.31) then becomes:

$$\begin{bmatrix} T_a \\ T_b \end{bmatrix} = \frac{\sqrt{3} T_s |\vec{V}_{ref}|}{2 V_{dc}} \begin{bmatrix} \sin \frac{k\pi}{3} & -\cos \frac{k\pi}{3} \\ -\sin \frac{(k-1)\pi}{3} & \cos \frac{(k-1)\pi}{3} \end{bmatrix} \begin{bmatrix} \cos n\omega T_s \\ \sin n\omega T_s \end{bmatrix}. \tag{3.32}$$

The modulation index is defined in Equation (3.18) as the ratio of the desired peak fundamental magnitude to the maximum fundamental output in a six-step mode:

$$MI = \frac{|\overrightarrow{V}_{ref}|}{V_{max_{sixstep}}} = \frac{\pi V_{ref}}{2V_{dc}} \tag{3.33}$$

or

$$|\overrightarrow{V}_{ref}| = MI\frac{2}{\pi}V_{dc}. \tag{3.34}$$

Substituting this equation into the above equation for T_a and T_b leads to the following duration times:

$$\begin{bmatrix} T_a \\ T_b \end{bmatrix} = \frac{MI\sqrt{3}T_s}{\pi} \begin{bmatrix} \sin\frac{k\pi}{3} & -\cos\frac{k\pi}{3} \\ -\sin\frac{(k-1)\pi}{3} & \cos\frac{(k-1)\pi}{3} \end{bmatrix} \begin{bmatrix} \cos n\omega T_s \\ \sin n\omega T_s \end{bmatrix}. \tag{3.35}$$

Since the sum of $2T_a$ and $2T_b$ should be less than or equal to T_s, the inverter has to stay in a zero state for the rest of the period. The duration of the null vectors is the remaining time in the switching period. Since

$$T_s = T_0 + 2(T_a + T_b) \tag{3.36}$$

then the time interval for the zero voltage vectors is

$$T_0 = T_s - 2(T_a + T_b). \tag{3.37}$$

The switching times are arranged symmetrical around the center of the switching period as shown in Figure 3.7. The zero vector $\overrightarrow{V}_7$ (1,1,1) is placed at the center of the switching period, and the zero vector $\overrightarrow{V}_0$ (0,0,0) at the start and the end, and the total period for a zero vector is divided equally among the two zero vectors.

In the under-modulation region, as the modulation index increases, the reference voltage vector grows outward in magnitude. It reaches the inscribed circle of the hexagon and T_0 will reduce to zero whenever the tip of the reference voltage vector is on the hexagon. If

the modulation index increases further, then T_0 becomes negative and meaningless. Therefore, the modulation index will reach a maximum of 0.907 in the linear under-modulation region.

The calculated values of T_a and T_b in term of T_s/V_{dc} for all six sectors are listed in Table 3.5. The time durations of two adjacent nonzero vectors in each sector are calculated

Table 3.5: Time Intervals T_a and T_b for Each Sector

Sector	θ	T_a	T_b
1	$0 < \theta \leq 60^o$	$\frac{3V_\alpha}{4} - \frac{\sqrt{3}V_\beta}{4}$	$0V_\alpha + \frac{\sqrt{3}V_\beta}{2}$
2	$60 < \theta \leq 120^o$	$\frac{3V_\alpha}{4} + \frac{\sqrt{3}V_\beta}{4}$	$\frac{-3V_\alpha}{4} + \frac{\sqrt{3}V_\beta}{4}$
3	$180 < \theta \leq 240^o$	$0V_\alpha + \frac{\sqrt{3}V_\beta}{2}$	$\frac{-3V_\alpha}{4} - \frac{\sqrt{3}V_\beta}{4}$
4	$120 < \theta \leq 180^o$	$\frac{-3V_\alpha}{4} + \frac{\sqrt{3}V_\beta}{4}$	$0V_\alpha - \frac{\sqrt{3}V_\beta}{2}$
5	$240 < \theta \leq 300^o$	$\frac{-3V_\alpha}{4} - \frac{\sqrt{3}V_\beta}{4}$	$\frac{3V_\alpha}{4} - \frac{\sqrt{3}V_\beta}{4}$
6	$180 < \theta \leq 240^o$	$0V_\alpha - \frac{\sqrt{3}V_\beta}{2}$	$\frac{3V_\alpha}{4} + \frac{\sqrt{3}V_\beta}{4}$

based on the magnitude and phase of the reference voltage. From Figure 3.7, a zero state vector is applied followed with two adjacent active vectors in half of the switching period. The next half of the switching period is symmetrical to the first half.

To generate the signals that produce the rotating vector, an equation is required to determine the time intervals for each sector. Figure 3.8 shows the pulse patterns generated by space vector PWM in sector 1.

For example [19], when $\overrightarrow{V}_{ref}$ is in sector 1 as shown in Figures 3.7 and 3.8, the $\overrightarrow{V}_1$ vector is applied to the inverter during T_a interval, and consequently the vector $\overrightarrow{V}_2$ is applied during T_2 interval. The PWM period is shared between $\overrightarrow{V}_1$ and $\overrightarrow{V}_2$ for durations T_a and T_b, respectively, and the zero vectors $\overrightarrow{V}_0$ and $\overrightarrow{V}_7$ for a duration T_0. The switching sequence is given by $\overrightarrow{V}_0$-$\overrightarrow{V}_1$-$\overrightarrow{V}_2$-$\overrightarrow{V}_7$-$\overrightarrow{V}_7$-$\overrightarrow{V}_2$-$\overrightarrow{V}_1$-$\overrightarrow{V}_0$ during two half-sampling periods. The generated space vector PWM waveforms are symmetrical with respect to the middle
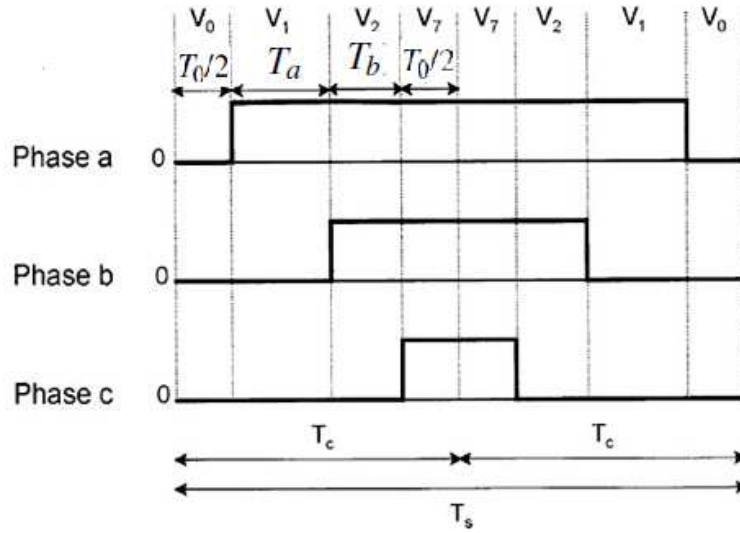
Figure 3.7: Construction of Symmetrical Pulse Pattern for Three-Phase [20].

of each PWM period. The switching frequency is the same as the sampling frequency of the inverter. An example of a symmetric space vector PWM waveform is shown in Figure 3.7 where it is assumed that the reference voltage is in the sector formed by vector $\vec{V}_1$ and $\vec{V}_2$ with angle $0 < \theta \le 60^o$. In Figure 3.7, switching states are required to change from one state to the next. The progress of switching states from the left to the right of that figure with following steps:

1. When the circuit configuration is in the $\vec{V}_0$ state (time interval is $T_0/2$), all top switches (S_1, S_3, and S_5) of Figure 3.2 are opened.

2. When it is in the $\vec{V}_1$ state (with a time interval T_a), switch S_1 is closed.

3. When it is in the $\vec{V}_2$ state (with a time interval T_b), switch S_3 is closed (S_1 is still closed).

4. When it is in the $\vec{V}_7$ state (with a time interval $T_0/2$), switch S_5 is closed. (S_1, and S_3, are still closed.)

After the first half of the switching period is done, the switching combination is reversed. All switches are closed for $T_0/2$ seconds before the circuit configuration is back to $\vec{V}_2$, then $\vec{V}_1$, and $\vec{V}_0$ with corresponding time intervals of T_b, T_a, and $T_0/2$. Following a similar process, the switching cycles are determined for the five remaining vectors.

From Tables 3.1 and 3.2 for this example the magnitude of all the space vectors is $2V_{dc}/3$ and the phase voltages are $V_{an} = 2V_{dc}/3$, $V_{bn} = -V_{dc}/3$, $V_{cn} = -V_{dc}/3$ and the line-to-line voltages are $V_{ab} = V_{dc}$, $V_{bc} = 0$, $V_{ca} = -V_{dc}$.
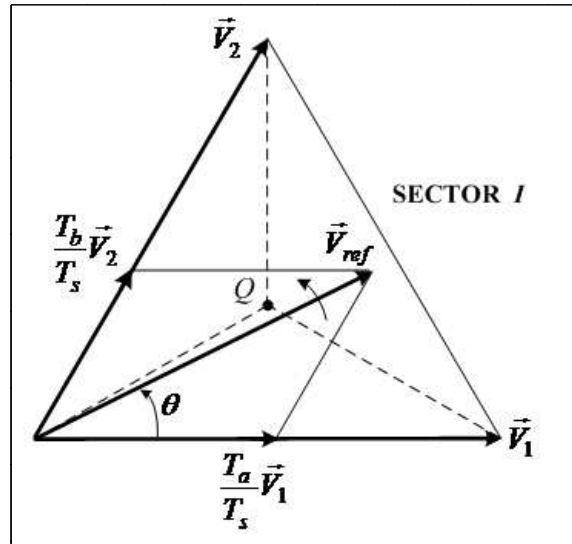
Figure 3.8: V_{ref} Falls into Sector 1 [21].

3.3.5 Determination of the Switching Times for Each Transistor Switch (S_1 - S_6)

It is necessary to arrange the switching sequence so that the switching frequency of each inverter leg is minimized. There are many switching patterns that can be used to implement SVPWM. To minimize the switching losses, only two adjacent active vectors and two zero vectors are used in a sector [15,20,21]. To meet this optimal condition, each switching period starts with one zero vector and end with another zero vector during the sampling time T_s. This rule applies normally to three-phase inverters as a switching sequence.

Therefore, the switching cycle of the output voltage is double the sampling time, and the two output voltage waveforms become symmetrical during T_s. Table 3.6 presents a symmetric switching sequence.

Referring to this table, the binary representations of two adjacent basic vectors differ in only one bit, so that only one of the upper transistors switches is closed when the switching pattern moves from one vector to an adjacent one. The two vectors are time-weighted in a sample period T_s to produce the desired output voltage.

Table 3.6: Seven-Segment Switching Sequence

Sector	Switching Segment						
	1	2	3	4	5	6	7
1	$\vec{V}_0$,[000]	$\vec{V}_1$,[100]	$\vec{V}_2$,[110]	$\vec{V}_7$,[111]	$\vec{V}_2$,[110]	$\vec{V}_1$,[100]	$\vec{V}_0$, [000]
2	$\vec{V}_0$,[000]	$\vec{V}_3$,[010]	$\vec{V}_2$,[110]	$\vec{V}_7$,[111]	$\vec{V}_2$,[110]	$\vec{V}_3$,[010]	$\vec{V}_0$, [000]
3	$\vec{V}_0$,[000]	$\vec{V}_3$,[010]	$\vec{V}_4$,[011]	$\vec{V}_7$,[111]	$\vec{V}_4$,[011]	$\vec{V}_3$,[010]	$\vec{V}_0$, [000]
4	$\vec{V}_0$,[000]	$\vec{V}_5$,[001]	$\vec{V}_4$,[011]	$\vec{V}_7$,[111]	$\vec{V}_4$,[011]	$\vec{V}_5$,[001]	$\vec{V}_0$, [000]
5	$\vec{V}_0$,[000]	$\vec{V}_5$,[001]	$\vec{V}_6$,[101]	$\vec{V}_7$,[111]	$\vec{V}_6$,[101]	$\vec{V}_5$,[001]	$\vec{V}_0$, [000]
6	$\vec{V}_0$,[000]	$\vec{V}_1$,[100]	$\vec{V}_6$,[101]	$\vec{V}_7$,[111]	$\vec{V}_6$,[101]	$\vec{V}_1$,[100]	$\vec{V}_0$, [000]

3.3.6 Types of Different Schemes

There are two modes of operation available for the PWM waveform: symmetric and asymmetric PWM. The pulse of an asymmetric edge aligned signal always has the same side aligned with one end of each PWM period. On the other hand, the pulse of symmetric signals is always symmetric with respect to the center of each PWM period. The symmetrical PWM signal is often preferred because it has been shown to have the lowest total harmonic distortion (THD), and has been implemented in [22,23,24]. Output patterns for each sector are based on a symmetrical sequence. There are different schemes in space

vector PWM and they are based on their repeating duty distribution. The seven-segment technique is studied in this thesis and will be referred to as the symmetric technique.

Based on the equations for T_a, T_b, T_0, T_7, and according to the principle of symmetrical PWM, the switching sequence in Table 3.7 is shown for the upper and lower switches.

Figure 3.10 shows the switching patterns of all six sectors in the circle. As shown in the same figure, the space vector for a three-phase voltage source inverter is divided into six sectors based on six fundamental vectors. Any voltage vector in this vector space can be synthesized using two adjacent vectors. One switching period is depicted in the same figure. In sector 1, for example, switching is achieved by applying a zero state vector followed by two adjacent active state vectors in a half switching period. The next half of the switching period is the mirror image of the first half.

In order to reduce the switching loss of the power components of the inverter, it is required that at each time only one bridge arm is switched. After re-organizing the switching sequences, a scheme with center-aligned pulses is obtained as shown in Figure 3.9.

The switching pulse patterns of six different sectors in Figure 3.11 are shown for the upper and lower switches of a three-phase inverter. It is obvious that in the odd sector the active state sequence is in ascending-descending order; whereas, it is in a descending-ascending order in an even sector. For example:

1. In an odd sector 1, the state sequence of space vectors is in the order $\vec{V}_0, \vec{V}_1, \vec{V}_2, \vec{V}_7, \vec{V}_7, \vec{V}_2, \vec{V}_1, \vec{V}_0$.

2. In an even sector 2, the state sequence of space vectors is: $\vec{V}_0, \vec{V}_3, \vec{V}_2, \vec{V}_7, \vec{V}_7, \vec{V}_2, \vec{V}_3, \vec{V}_0$.

Following the same procedure, we have the switching sequence summarized in Table 3.8 for all six sectors.
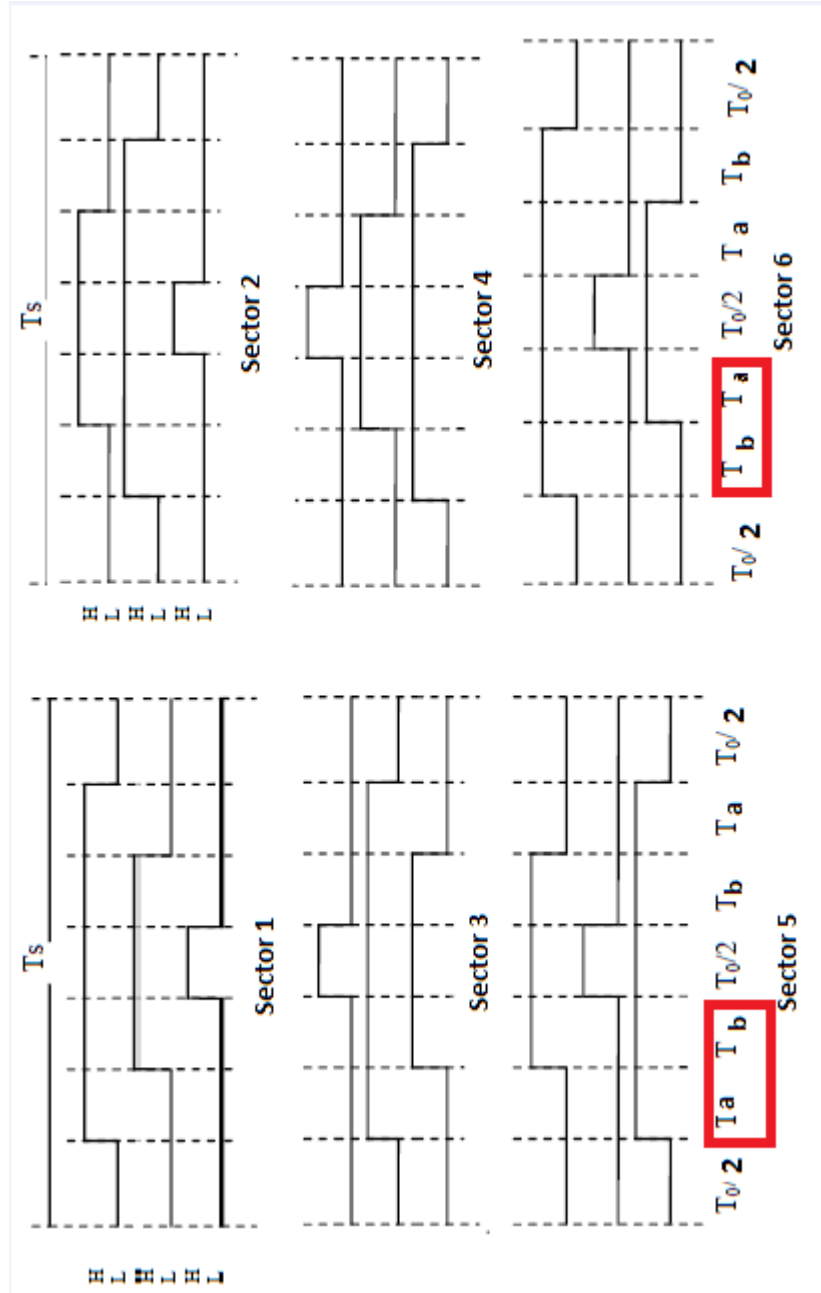
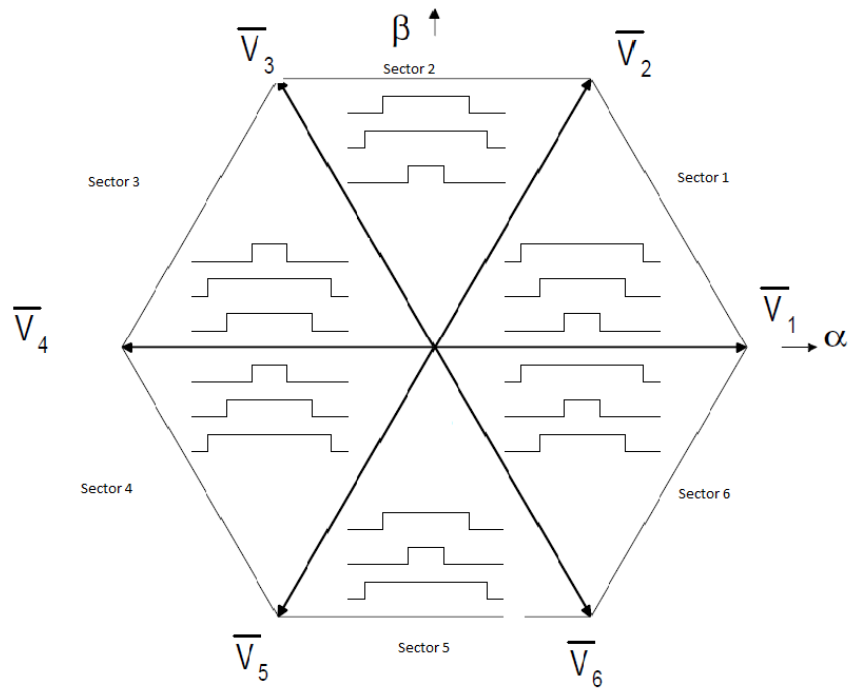Figure 3.9: Switching Patterns in the Six Sectors [20].

Figure 3.10: Switching Patterns of Six Sectors in Circle [20].

Table 3.7: Switching Pulse Pattern for the Three Phase for Each Sector

Sector	Upper Switches: S1, S3, S5	Lower Switches: S4, S6, S2
1	$S_1 = T_a + T_b + T_0/2$ $S_3 = T_b + T_0/2$ $S_5 = T_0/2$	$S_4 = T_0/2$ $S_6 = T_a + T_0/2$ $S_2 = T_a + T_b + T_0/2$
2	$S_1 = T_a + T_0/2$ $S_3 = T_a + T_b + T_0/2$ $S_5 = T_0/2$	$S_4 = T_b + T_0/2$ $S_6 = T_0/2$ $S_2 = T_a + T_b + T_0/2$
3	$S_1 = T_0/2$ $S_3 = T_a + T_b + T_0/2$ $S_5 = T_b + T_0/2$	$S_4 = T_a + T_b + T_0/2$ $S_6 = T_0/2$ $S_2 = T_a + T_0/2$
4	$S_1 = T_0/2$ $S_3 = T_a + T_0/2$ $S_5 = T_a + T_b + T_0/2$	$S_4 = T_a + T_b + T_0/2$ $S_6 = T_b + T_0/2$ $S_2 = T_0/2$
5	$S_1 = T_b + T_0/2$ $S_3 = T_0/2$ $S_5 = T_a + T_b + T_0/2$	$S_4 = T_a + T_0/2$ $S_6 = T_a + T_b + T_0/2$ $S_2 = T_0/2$
6	$S_1 = T_a + T_b + T_0/2$ $S_3 = T_0/2$ $S_5 = T_a + T_0/2$	$S_4 = T_0/2$ $S_6 = T_a + T_b + T_0/2$ $S_2 = T_b + T_0/2$

Table 3.8: Switching Sequence for Three-Phase PWM Technique

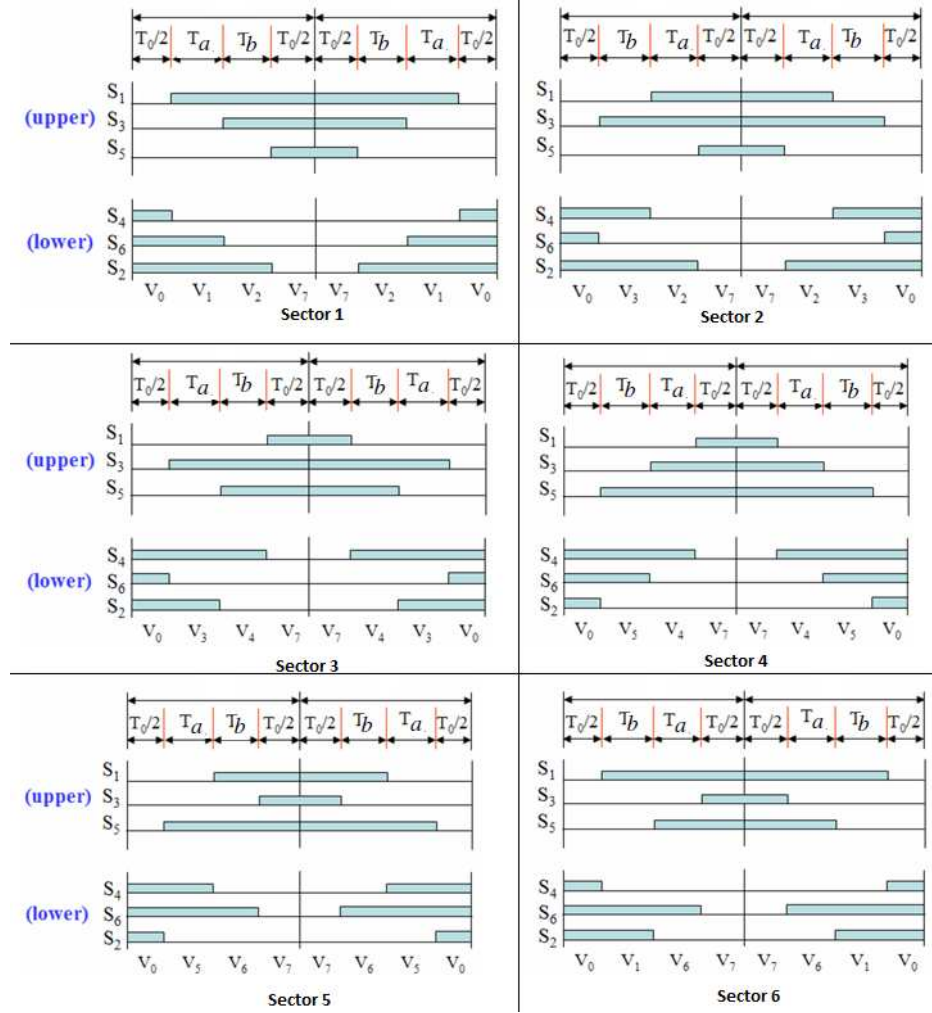| Sector	Switching Sequence of the Three Phase Modulation
1	$\vec{V}_0$-$\vec{V}_1$-$\vec{V}_2$-$\vec{V}_7$-$\vec{V}_2$-$\vec{V}_1$-$\vec{V}_0$
2	$\vec{V}_0$-$\vec{V}_3$-$\vec{V}_2$-$\vec{V}_7$-$\vec{V}_2$-$\vec{V}_3$-$\vec{V}_0$
3	$\vec{V}_0$-$\vec{V}_3$-$\vec{V}_4$-$\vec{V}_7$-$\vec{V}_4$-$\vec{V}_3$-$\vec{V}_0$
4	$\vec{V}_0$-$\vec{V}_5$-$\vec{V}_4$-$\vec{V}_7$-$\vec{V}_4$-$\vec{V}_5$-$\vec{V}_0$
5	$\vec{V}_0$-$\vec{V}_5$-$\vec{V}_6$-$\vec{V}_7$-$\vec{V}_6$-$\vec{V}_5$-$\vec{V}_0$
6	$\vec{V}_0$-$\vec{V}_1$-$\vec{V}_6$-$\vec{V}_7$-$\vec{V}_6$-$\vec{V}_1$-$\vec{V}_0$

Figure 3.11: Switching Sequence of all Six Sectors [4].

CHAPTER 4

SPACE VECTOR PWM IN OVER-MODULATION REGION

4.1   Introduction

Full utilization of the DC bus voltage is important for achieving, for example, maximum output torque under all operating conditions in AC machine drive applications. Over-modulation aims to extend the linear operation region of the SVPWM, which leads to a better utilization of the DC bus voltage and enhances the power utilization of the voltage source inverter. Several approaches to over-modulation have been proposed to extend the linear region of SVPWM over the years. It is an advanced method and possibly the best technique for variable frequency drive applications.

For SPWM, the highest possible peak phase fundamental voltage is $0.5V_{dc}$. With SVPWM, the peak phase fundamental voltage can be as high as $0.577V_{dc}$ during under-modulation when the reference vector makes a circular trajectory and it can be higher in the nonlinear modulation region when the desired trajectory partly passes outside of the hexagon.

The modulation index of the over-modulation region ranges from 0.907 up to 1 [11]. The over-modulation range can be considered as one region or it can be divided into two regions (see Figure 4.1). In this thesis, the over-modulation region is considered as two regions with two modes of operation depending on the modulation index values.

- In mode 1, the actual voltage vector keeps the angular speed of a modified reference vector constant, but its amplitude changes over time.
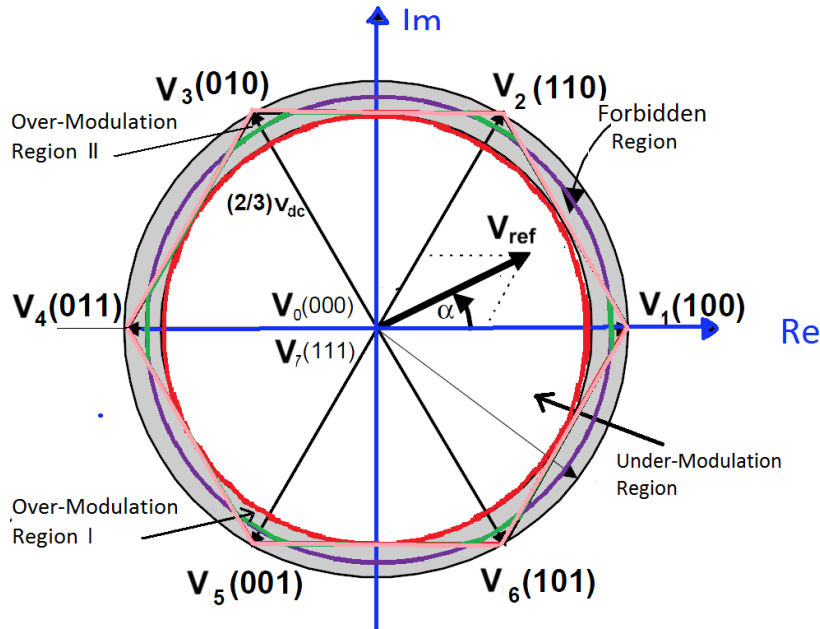
Figure 4.1: The Two Over-Modulation Regions in Space Vector Representation [12].

- In mode 2, both the amplitude and angle of the modified reference vector are varied.

4.2   Over-Modulation Mode 1

The over-modulation region starts when the reference voltage exceeds the hexagon boundary, and the MI is larger than 0.907. The boundary between the under-modulation zone and over-modulation region 1 starts when MI=0.907 and the boundary between the over-modulation region 1 and the over-modulation region 2 starts when MI=0.952. In region 1, the crossover angle (α_r) is measured from a hexagon vertex to the intersection of the compensated voltage vector trajectory with a hexagon side (see Figure 4.3). The crossover angle decreases as the modulation index is increased until at the limit of region 1. It depends on the value of the modulation index and varies between $\pi/6$ at the beginning of region 1 when MI=0.907 and 0° at the end of region 1 when MI =0.952 as shown in Figure 4.2. When the crossover angle equals zero degrees, the reference vector is fully on

the hexagon. The fundamental peak value generated in this way voltage is about 95% of the peak voltage of the square wave. This gives a modulation index of 0.952 [23].
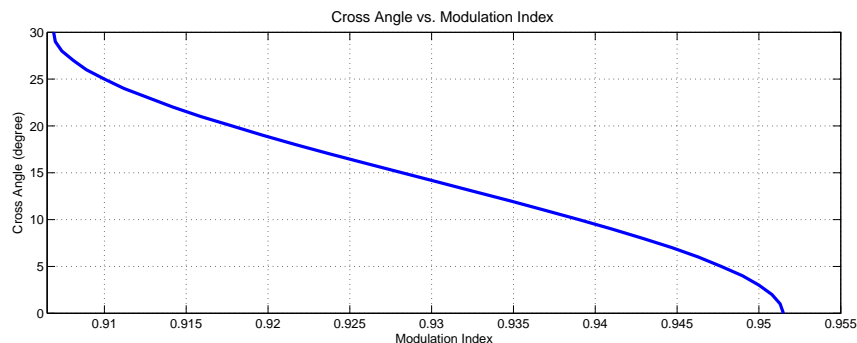

Figure 4.2: Crossover Angle vs. Modulation Index in the Mode 1.

In mode 1, the amplitude of the desired voltage is modified to fit inside a hexagon while the desired phase angle is not modified. It starts when the reference voltage $\overrightarrow{V}_{ref}$ crosses the hexagon at two points in each sector. Figure 4.3 shows two crossing points at B and C. There is a loss of fundamental voltage in the region where the reference vector exceeds the hexagon boundary of B-C. To compensate for that loss, the output voltage must track the modified reference voltage $\overrightarrow{V}_{ref}$, where it must change to a larger radius. This leads to a new reference voltage ($\overrightarrow{V}'_{ref}$), which crosses the hexagon at an angle α_r. The angle of the new reference vector is transmitted without any change.

The characteristic of the over-modulation mode 1 is that the voltage space vector moves partially on the hexagon (along B-C) and partially on the circle providing a continuous operation. The output voltage waveform is approximated by linear segments on the hexagon trajectory and by sinusoidal segments on the circular trajectory.

When the reference voltage vector is within the hexagon, near the outer corners of a sector on curve length A-B in the same figure, it is on a circular trajectory with switching times of T_a, T_b, and T_0 as in the under-modulation mode, but with a modified reference voltage.

During the nonlinear modulation, only the active vectors are taken into account while
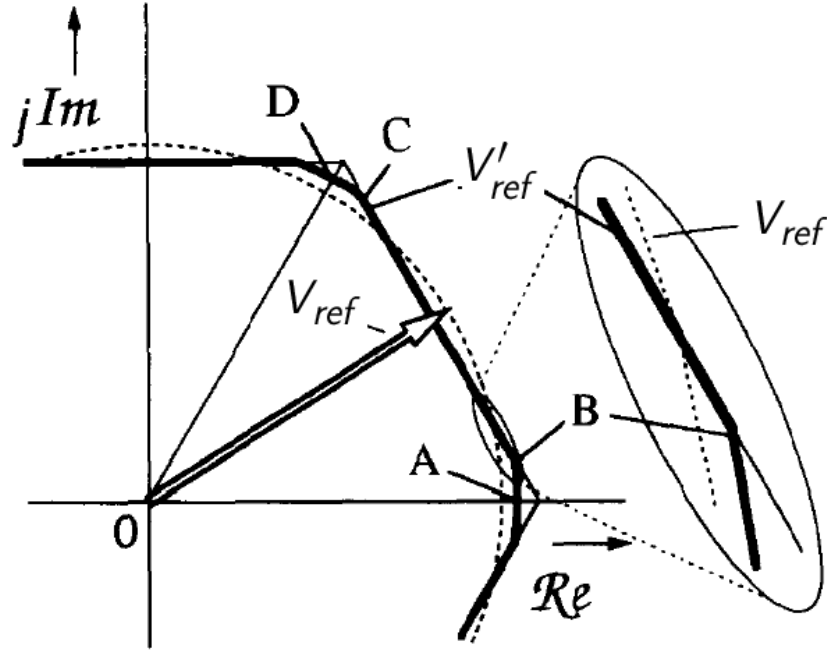
Figure 4.3: Over-Modulation Mode Region 1 [12].

the zero states are neglected. So, when $\overrightarrow{V}_{ref}$ is on the hexagon, $T_0'=0$, the switching times must be calculated using the modified equations [10]:

$$T_a' = \left[\frac{T_s}{2}\right]\frac{T_a}{T_a+T_b} \tag{4.1}$$

$$T_b' = \left[\frac{T_s}{2}\right]\frac{T_b}{T_a+T_b}. \tag{4.2}$$

When the original reference trajectory passes outside of the hexagon, the tip of the reference vector is located in the area between the inside circle and the outside circle of the hexagon. The T_a and T_b equations in linear space vector PWM yield a negative and meaningless duration for the zero vectors. Whether the trajectory is inside the hexagon or not can be easily recognized using the following explanation.

The magnitude of the new reference voltage is a function of the phase angle θ. If the modulation index is above 0.907, the desired trajectory passes outside of the hexagon and the interval time T_0 is negative on the zero state vectors. In this case, the converter exceeds its linear region of operation and enters the over-modulation region. Therefore, the synthesized waveform becomes distorted.

If T_0' is equal to zero, T_a' and T_b' should be reduced with an equal ratio so that their sum should equal T_s. We need to use Equations (4.1) and (4.2) for T_a' and T_b' in the region where the modified reference trajectory moves along the hexagon. The durations of the active vectors during one switching period T_s are calculated using

$$T_a' = \left[\frac{T_s}{2}\right] \frac{\sqrt{3}\cos(\alpha - (k-1)\frac{\pi}{3}) - \sin(\alpha - (k-1)\frac{\pi}{3})}{\sqrt{3}\cos(\alpha - (k-1)\frac{\pi}{3}) + \sin(\alpha - (k-1)\frac{\pi}{3})} \tag{4.3}$$

$$T_b' = T_s - T_a' \tag{4.4}$$

$$T_0' = 0, \tag{4.5}$$

where k is the sector number. Equation (4.3) to (4.5) are used to calculate the durations of the active vectors for each sector. Table 5.1 shows those durations for each sector. Using

Table 4.1: The Time Intervals T_a' and T_b' for Each Sector

Sector	θ	T_a'	T_b'
1	$0 < \theta \le 60^0$	$\frac{\sqrt{3}V_\alpha - V_\beta}{\sqrt{3}V_\alpha + V_\beta}$	$\frac{2V_\beta}{\sqrt{3}V_\alpha + V_\beta}$
2	$60 < \theta \le 120^0$	$\frac{\sqrt{3}V_\alpha + V_\beta}{2V_\beta}$	$\frac{-\sqrt{3}V_\alpha + V_\beta}{2V_\beta}$
3	$120 < \theta \le 180^0$	$\frac{2V_\beta}{-\sqrt{3}V_\alpha + V_\beta}$	$\frac{-\sqrt{3}V_\alpha - V_\beta}{-\sqrt{3}V_\alpha + V_\beta}$
4	$180 < \theta \le 240^0$	$\frac{-\sqrt{3}V_\alpha + V_\beta}{-\sqrt{3}V_\alpha - V_\beta}$	$\frac{-2V_\beta}{-\sqrt{3}V_\alpha - V_\beta}$
5	$240 < \theta \le 300^0$	$\frac{-\sqrt{3}V_\alpha - V_\beta}{-2V_\beta}$	$\frac{\sqrt{3}V_\alpha - V_\beta}{-2V_\beta}$
6	$300 < \theta \le 360^0$	$\frac{-2V_\beta}{\sqrt{3}V_\alpha - V_\beta}$	$\frac{\sqrt{3}V_\alpha + V_\beta}{\sqrt{3}V_\alpha - V_\beta}$

Equation (3.22) in the under-modulation chapter, we can find the new reference voltage space vector in the over-modulation region of mode 1:

$$\overrightarrow{V}_{ref}\frac{T_s}{2} = \overrightarrow{V}_k.T_a + \overrightarrow{V}_{k+1}.T_b. \tag{4.6}$$

Then,

$$
\begin{aligned}
\overrightarrow{V}'_{ref}\frac{T_s}{2} &= \overrightarrow{V}_k T'_a + \overrightarrow{V}_{k+1} T'_b \\
\overrightarrow{V}'_{ref} &= \left[\frac{2}{T_s}\right]\left(\overrightarrow{V}_k T_a + \overrightarrow{V}_{k+1} T_b\right)\left(\frac{T_s}{2(T_a + T_b)}\right) \\
\overrightarrow{V}'_{ref} &= \left(\frac{T_s}{2(T_a + T_b)}\right)\overrightarrow{V}_{ref}.
\end{aligned}
\tag{4.7}
$$

Referring to Figure 4.4, consider the trajectory of three voltage vectors rotating in a complex plane (left-hand side) and the phase voltage waveform of an actual voltage reference vector transformed in a time domain (right-hand side), which is actually modulated by the inverter [14]. The phase voltage waveform is divided into four segments and the
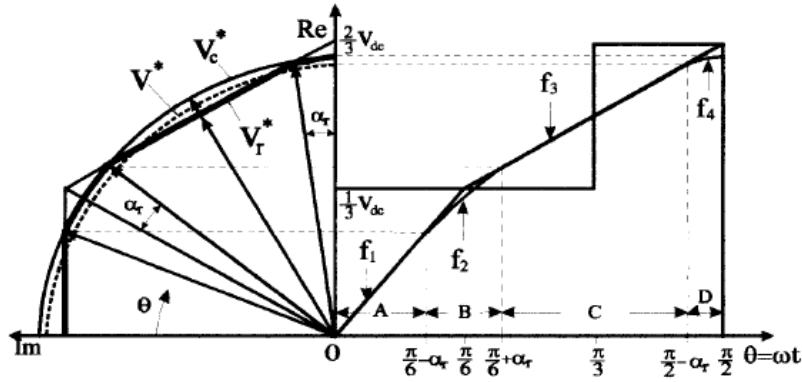

Figure 4.4: Trajectory of Reference Voltage Vector and Phase Voltage Waveform in Mode 1 [14].

voltage equations in each segment are expressed as follows [14]:

$$
\begin{aligned}
f_1 &= \frac{V_{dc}}{\sqrt{3}}\tan\theta, & &\text{for} & (\frac{\pi}{6}-\alpha_r) > \theta \geq 0 \\[2mm]
f_2 &= \frac{V_{dc}}{\sqrt{3}\cos(\frac{\pi}{6}-\alpha_r)}\sin\theta, & &\text{for} & (\frac{\pi}{6}+\alpha_r) > \theta \geq (\frac{\pi}{6}-\alpha_r) \\[2mm]
f_3 &= \frac{V_{dc}}{\sqrt{3}\cos(\frac{\pi}{3}-\alpha_r)}\sin\theta, & &\text{for} & (\frac{\pi}{2}-\alpha_r) > \theta \geq (\frac{\pi}{6}+\alpha_r) \\[2mm]
f_4 &= \frac{V_{dc}}{\sqrt{3}\cos(\frac{\pi}{6}-\alpha_r)}\sin\theta, & &\text{for} & (\frac{\pi}{2}) > \theta \geq (\frac{\pi}{2}-\alpha_r),
\end{aligned}
\tag{4.8}
$$

where $\theta = \omega t$ and ω is the angular velocity of the fundamental voltage reference vector.

The modification of the reference voltage vector is the same in all of the six sectors of vector diagram, the relationship between the crossover angle (α_r) and the new reference voltage is given by:

$$
\cos(\frac{\pi}{6}-\alpha_r) = \frac{(V_{dc}/\sqrt{3})}{(\overrightarrow{V}'_{ref})}.
\tag{4.9}
$$

By expanding those four segment equations with a Fourier series, the fundamental component of the phase voltage can be expressed as:

$$
F(\alpha_r) = \frac{4}{\pi}\left[\int_0^{\frac{\pi}{6}-\theta} f_1\sin\theta d\theta + \int_{\frac{\pi}{6}-\theta}^{\frac{\pi}{6}+\theta} f_2\sin\theta d\theta + \int_{\frac{\pi}{6}+\theta}^{\frac{\pi}{2}-\theta} f_3\sin\theta d\theta \int_{\frac{\pi}{2}-\theta}^{\frac{\pi}{2}} f_4\sin\theta d\theta\right]
\tag{4.10}
$$

This integral ranges from an angle of 0 to $\pi/2$ as shown in the complex plane (right part) of the same figure. We can obtain the value of Fourier series $F(\alpha_r)$ with respect to the angle α_r. Since $F(\alpha_r)$ is the peak of the reference voltage,

$$
F(\alpha_r) = \frac{2}{\pi}V_{dc}\times MI
\tag{4.11}
$$

and according to the definition of the modulation index,

$$MI = \frac{F(\alpha_r)}{\frac{2}{\pi}V_{dc}}.$$
(4.12)

The Fourier series $F(\alpha_r)$ can be generated from a MATLAB script. The relationship between MI and the angle α_r gives us the plot shown in Figure 4.2, which shows the correlation between MI and the crossover angle α_r.

4.3 Over-Modulation Mode 2

At the end of mode 1, the component of the reference voltage changes to a piecewise linear waveform. When the modulation index is higher than 0.952, the second region of the over-modulation region algorithm is entered. Both the reference magnitude and the phase angle have to be changed compared to the linear region. The modified reference vector is held at a vertex of the hexagon in every sector for the rest of the switching period. The angle for which the active switching state vector is held constant is called the holding angle α_h. Figure 4.5 shows the holding angle in region 2 as a function of the modulation index.
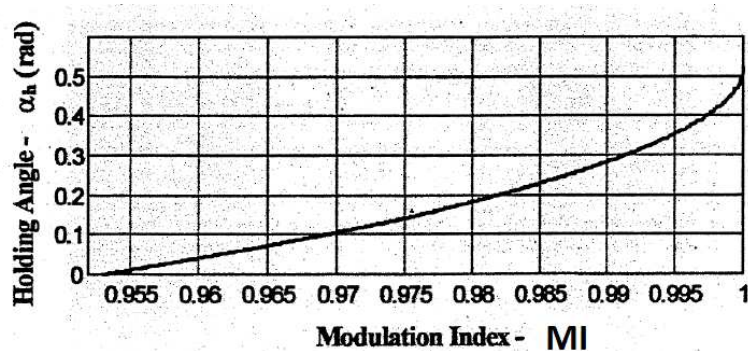

Figure 4.5: Holding Angle vs. Modulation Index in Mode 2 [11].

At the end of Mode 2, the linear segments vanish giving a six-step or square-wave operation where the modified vector is held at the hexagon corner for 60°, that is, $\alpha_h = 30^o$

[11]. An expression for the modified angle α_h in Mode 2 can be given as

$$
\alpha_m = \begin{cases} 0 & \text{if}: 0 \leq \alpha \leq \alpha_h \\ \frac{\alpha - \alpha_h}{\pi/6 - \alpha_h} * \frac{\pi}{6} & \text{if}: \alpha_h < \alpha < (\pi/3 - \alpha_h) \\ \frac{\pi}{3} & \text{if}: (\pi/3 - \alpha_h) \leq \alpha \leq \pi/3, \end{cases} \tag{4.13}
$$

α_m is the modified angle of α_h.

The holding angle increases from 0 to $\pi/6$ as modulation index goes from 0.955 to 1. The relation between the holding angle and the modulation index is nonlinear [16]. Therefore, the actual trajectory is modified so that the output fundamental voltage matches that of the reference voltage. The operation in this region is characterized by partly holding the modified vector at a hexagon corner for a holding angle α_h, and partly by tracking the hexagon sides in every sector. During the holding angle, the magnitude of V_{an} remains constant, whereas during hexagon tracking, the voltage changes almost linearly. In Figure 4.6, the trajectory shows five steps following by four angle ranges.
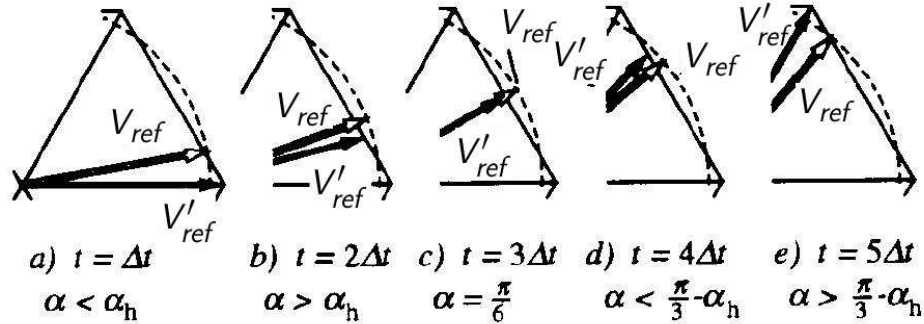

Figure 4.6: Angular Displacement of Reference and Actual Voltage Vectors in Mode 2 [12].

1. If the angle falls between zero and the holding angle (α_h), the modified reference voltage vector is held at a vertex, while the fundamental voltage vector is continu-

ously rotating.

2. If the angle range is from the holding angle to $(\pi/6\text{-}\alpha_h)$, the modified reference vector moves along the hexagon, but lags the fundamental voltage vector.

3. When α equals $\pi/6$ exactly, the modified reference vector catches up with the reference vector.

4. When $\alpha < (\frac{\pi}{3} - \alpha_h)$, the modified reference vector speeds past it until $\alpha = \pi/3 - \alpha_h$.

5. In the last angle range $(\pi/3 > \alpha \geq \pi/3 - \alpha_h)$, the modified reference voltage vector has just arrived at the other vertex. It remains there until the reference voltage vector has caught up with the modified reference voltage vector.

The modulation will gradually change to a six-step mode for α_h equal zero and generate a square wave when the modulation index gets close to 1. The six-step mode is characterized by a selection of the switching vector for one-sixth of the fundamental period. In this case, the maximum possible inverter output voltage is generated. Mode 2 ends when the holding angle is $\pi/6$.

The voltage equations in the four segments (see Figure 4.7) are expressed as:

$$
\begin{aligned}
f_1 &= \frac{V_{dc}}{\sqrt{3}}.\tan\alpha_p, && \text{for} && 0 \leq \theta < (\frac{\pi}{6} - \alpha_h) \\
f_2 &= \frac{V_{dc}}{3}, && \text{for} && (\frac{\pi}{6} - \alpha_h) \leq \theta < (\frac{\pi}{6} + \alpha_h) \\
f_3 &= \frac{V_{dc}\sin(\alpha'_p)}{\sqrt{3}.\cos(\frac{\pi}{3} - \alpha'_p)}, && \text{for} && (\frac{\pi}{6} + \alpha_h) \leq \theta < (\frac{\pi}{2} - \alpha_h) \\
f_4 &= \frac{2V_{dc}}{3}, && \text{for} && (\frac{\pi}{2} - \alpha_h) \leq \theta < \frac{\pi}{2})
\end{aligned}
\tag{4.14}
$$

where

$$
\alpha'_p = \alpha_p - \frac{6}{\pi} = \frac{\theta}{1 - \frac{6\alpha_h}{\pi}} - \frac{\pi}{6} = \frac{\theta - \frac{\pi}{6} + \alpha_h}{1 - \frac{6\alpha_h}{\pi}} = \frac{\theta' + \alpha_h}{1 - \frac{6\alpha_h}{\pi}}
\tag{4.15}
$$

Equations (4.10) to (4.12) are then used to find the values of modulation index and Fourier

series $F(\alpha_h)$ with respect to the holding angle. A relationship between MI and holding angle gives us the plot shown in Figure 4.5 [14]. The modulation index increases from 0 to $\pi/6$ as the holding angle increases from 0.955 to 1.
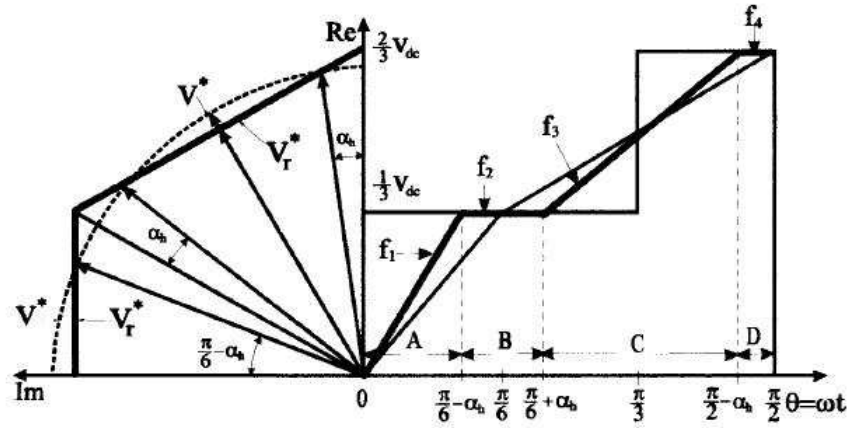

Figure 4.7: Trajectory of Reference Voltage Vector and Phase Voltage Waveform in Mode 2.

CHAPTER 5

SIMULATION RESULTS

5.1   Introduction

This chapter discusses the MATLAB/Simulink software implementation of SPWM, THIPWM, and SVPWM in the under-modulation region and the over-modulation region 1. We describe Simulink models built on the corresponding equations in previous chapters. In addition to the simulation results, this chapter includes detailed subsystems of the Simulink models as well as an explanation of the role of every subsystem. Low-pass filters are required at the outputs in order to filter out the PWM waveforms and visualize the fundamental results. Our simulation analysis does not include the programming of dead time for the switching of complementary switches in an inverter leg.

Simulation results are presented in three groups based on three simulation models. The first group (Figures 5.1-5.6) shows simulation results for SPWM and THIPWM. The second group (Figures 5.7-5.18) presents the under-modulation results for SVPWM. The third group shows the simulation results of region 1 in the over-modulation SVPWM (Figures 5.19-5.23).

The simulation of the over-modulation region 2 of SVPWM has been excluded from this thesis. A different method needs to be implemented that ensures that the output voltage varies continuously in this mode.

5.2   Sinusoidal PWM

SPWM is very popular and easy to implement using comparators. The SPWM simulink system model is built in Figure 5.1. It has the following blocks: (1) Sinusoidal wave generators, (2) High-frequency triangular wave generator, and (3) comparators.
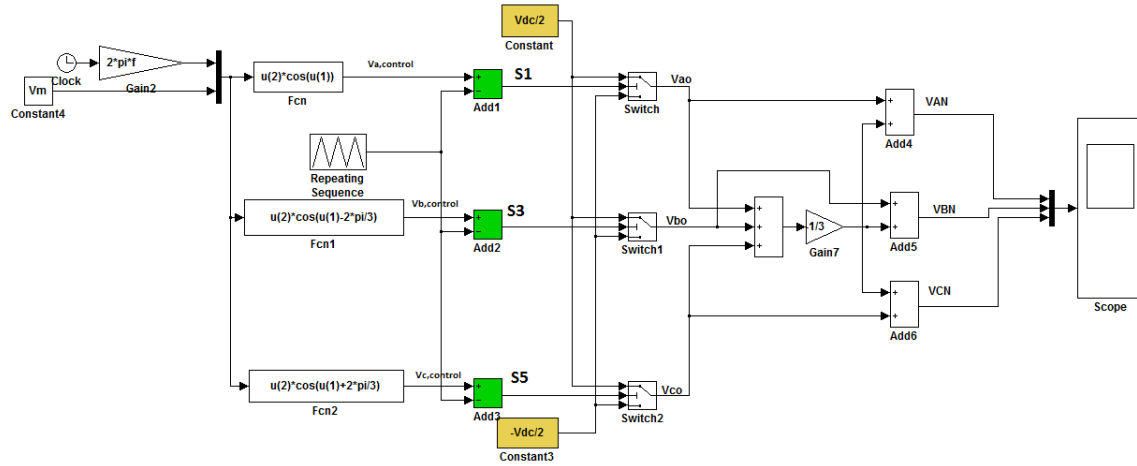

Figure 5.1: SPWM System Model.

The SPWM technique treats each modulating voltage as a separate entity that is compared to the common carrier triangular waveform. A three-phase voltage set (V_a, V_b, and V_c) of variable amplitude is compared in three separate comparators with a common triangular carrier waveform of fixed amplitude as shown in the same figure. The output (V_{ao}, V_{bo}, and V_{co}) of the comparators form the control signals for the three legs of the inverter composed of the switch pairs (S_1, S_4), (S_3, S_6), and (S_5, S_2), respectively. From these switching signals and the DC bus voltage, PWM phase-to-neutral voltages (V_{an}, V_{bn}, and V_{cn}) are obtained. In the simulink model, the simulation is performed under the following conditions:

$$V_{dc} \;=\; 300 \text{ V}$$

$$\text{Switching frequency} \;=\; 1800 \text{ Hz}$$

$$\text{Inverter frequency} \;=\; 60 \text{ Hz}$$

$$V_{ref} \;=\; 150 \text{ V}.$$
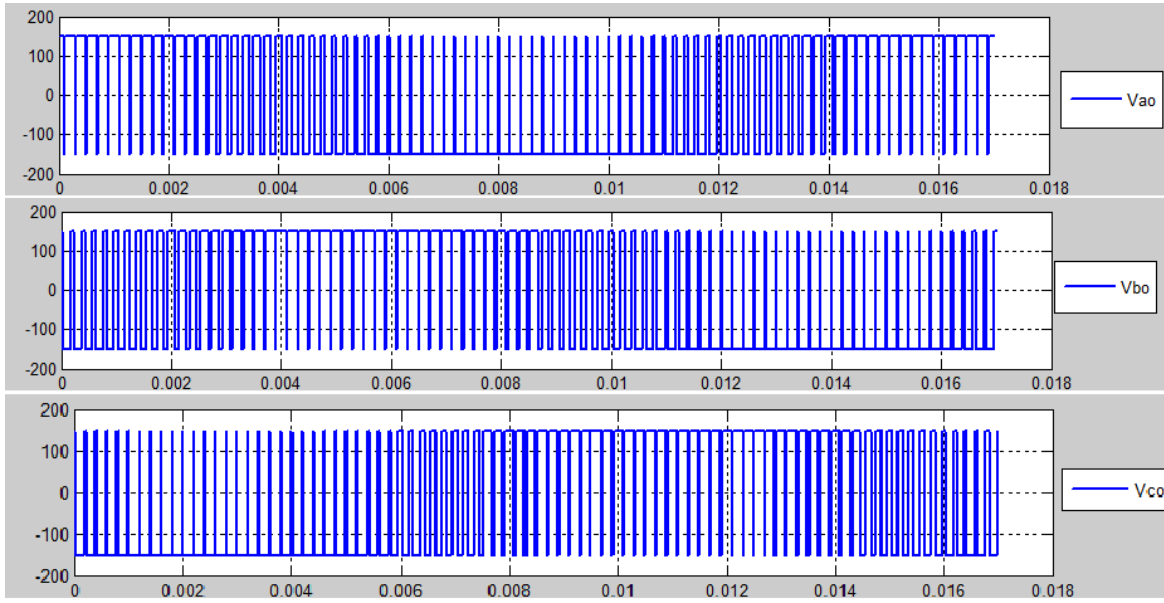
Figure 5.2: V_{ao}, V_{bo}, and V_{co} of SPWM Waveforms.

Figure 5.3 shows the simulated pole voltages V_{ao}, V_{bo}, and V_{co}. The relationship between the line-to-neutral voltages and the switching states (S_1, S_3, and S_5) in a balanced three-phase load are:

$$V_{an} \;=\; \frac{V_{dc}}{3}(2S_1 - S_3 - S_5)$$
$$V_{bn} \;=\; \frac{V_{dc}}{3}(-S_1 + 2S_3 - S_5)$$
$$V_{cn} \;=\; \frac{V_{dc}}{3}(-S_1 - S_3 + 2S_5).$$
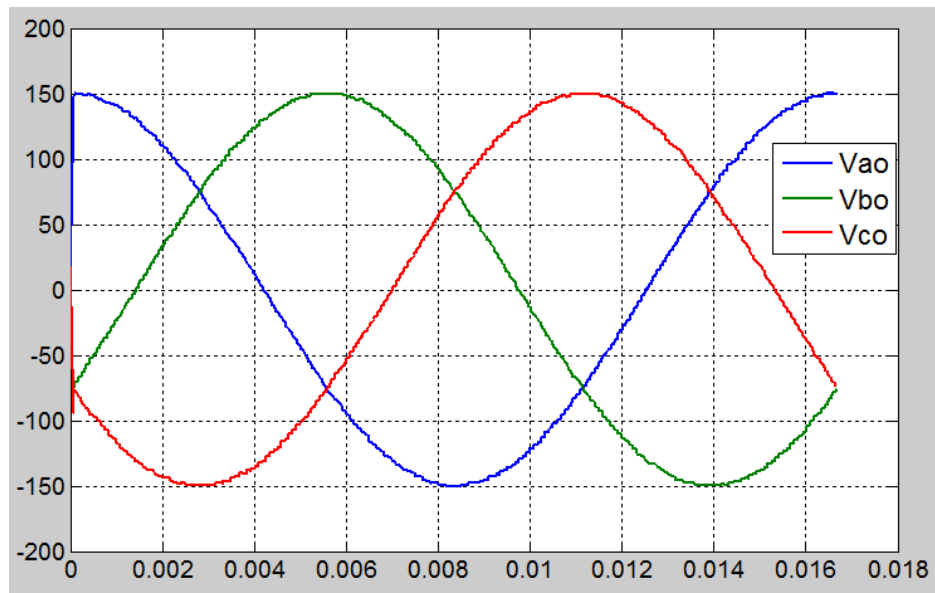
Figure 5.3: V_{ao}, V_{bo}, and V_{co} of SPWM after Filtering.

To visualize the actual results, filtering of the PWM waveforms is required. The line-to-neutral voltages V_{an}, V_{bn}, and V_{cn} are shown after they have been passed through a low-pass filter. As expected, magnitudes of the phase voltages (V_{an}, V_{bn}, and V_{cn}) are about $0.5V_{dc}$. The output voltage waveforms show that the higher the switching frequencies, the smoother the output voltage waveforms, as expected.

5.3   THIPWM

The THIPWM simulink system model is the same as that of the SPWM system except for the modulating waveform voltages, which are generated by injected the third-harmonic components as follows:

Figure 5.4: Neutral Voltages V_{an}, V_{bn}, and V_{cn} of SPWM after Filtering.
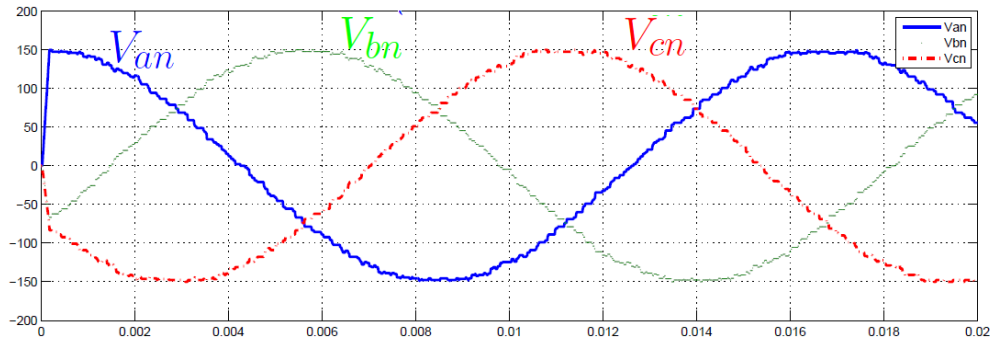
$$V_a = \frac{2}{\sqrt{3}}\left(\sin(\omega t) + \frac{1}{6}\sin(3\omega t)\right)$$

$$V_b = \frac{2}{\sqrt{3}}\left(\sin(\omega t - 2\pi/3) + \frac{1}{6}\sin(3\omega t)\right)$$

$$V_c = \frac{2}{\sqrt{3}}\left(\sin(\omega t + 2\pi/3) + \frac{1}{6}\sin(3\omega t)\right).$$

Figure 5.5 shows the line-to-neutral voltages and Figure 5.6 shows the line-to-line voltage of THIPWM. As expected, the magnitude of the phase voltage is about $300/\sqrt{(3)}$ (Volts) and 300 (Volts) for line-to-line voltage, and the results show that THIPWM improves the fundamental voltages compared to SPWM.

5.4   Under-Modulation of Space Vector PWM

A two-level three-phase inverter has eight possible inverter switching states that can generate eight space vectors: six non-zero vectors ($\overrightarrow{V}_1$ to $\overrightarrow{V}_6$) and two zero vectors ($\overrightarrow{V}_0$ and $\overrightarrow{V}_7$). These vectors are applied during the switching times T_a, T_b, and T_0. According to the time duration equations in the chapter on under-modulation SVPWM, the average pole voltage vector over one PWM period can be averaged using two adjacent vectors and the null vectors.
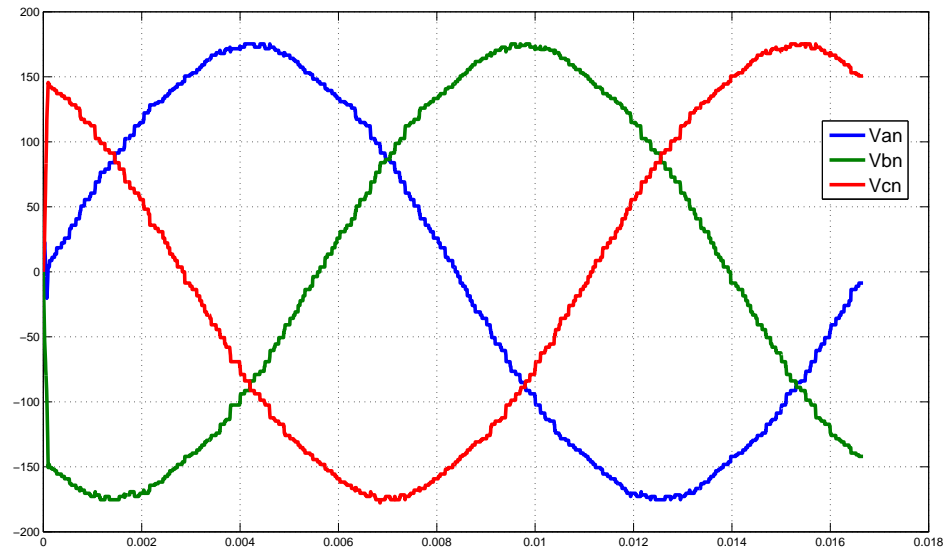
Figure 5.5: Neutral Voltages V_{an}, V_{bn}, and V_{cn} of THIPWM after Filtering.
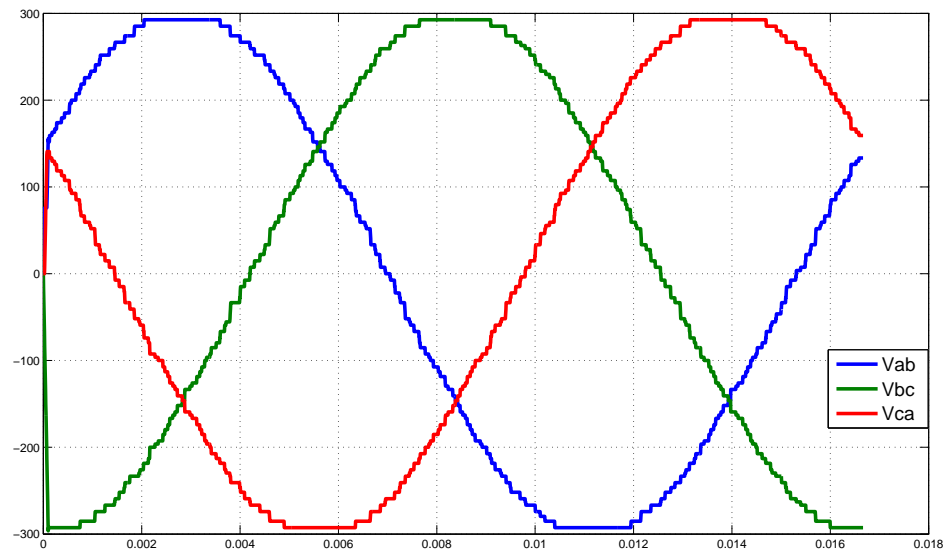

Figure 5.6: Neutral Voltages V_{ab}, V_{bc}, and V_{ca} of THIPWM after Filtering.

To generate a rotating space vector with constant amplitude, the reference voltage vector must be limited to the inscribed circle inside the hexagon. The simulation model used to verify the under-modulation SVPWM scheme is shown in Figure 5.7 and it has seven main subsystems or blocks, which are shown in detail in Figures 5.8-5.13.

1. The first block Figure 5.8 is used to generate three-phase sinusoidal input voltages with variable frequency, amplitude, direction, and DC bus voltage. The three signals are delayed by 120° from each other.

2. The three-phase abc voltages are then converted to two-phase $\alpha\beta$ voltages given in the second block as:

$$V_\alpha = \frac{2}{3}V_a - \frac{1}{3}V_b - \frac{1}{3}V_c$$
$$V_\beta = \frac{1}{\sqrt{3}}V_b - \frac{1}{\sqrt{3}}V_c.$$

It is necessary to know in which sector the reference output is in order to determine the switching time. The reference voltages V_α and V_β are utilized to determine the sector of the vectors from 1 to 6 as shown in Figure 5.9. These values are the inputs to the third block.

3. Equations (5.1) and (5.2) in the third block calculates the phase angle,

$$\theta = \tan^{-1}(\frac{V_\beta}{V_\alpha}) \tag{5.1}$$
$$\theta \in [0, 2\pi] \tag{5.2}$$

and using Table 3.5, it can be used to identify the sector of the reference voltage as shown in Figure 5.10.

The modulation index is entered in the first block. It is the ratio of the amplitude of the output sinusoidal voltage to the maximum fundamental voltage.
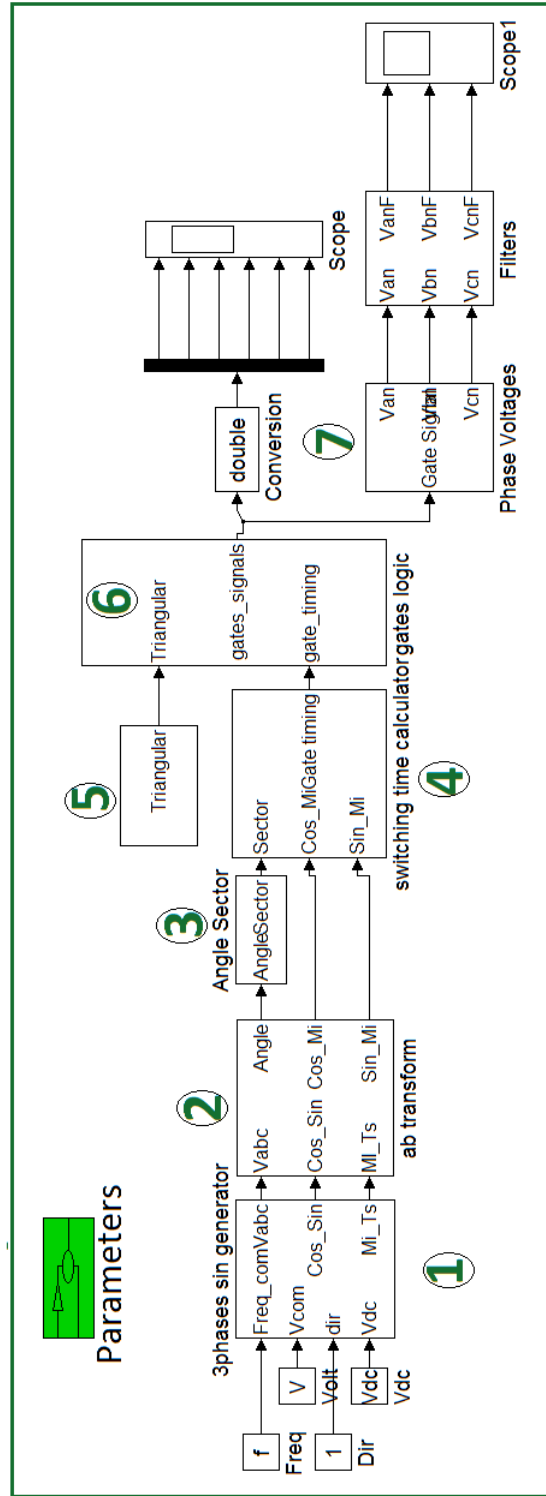
Figure 5.7: Linear Modulation of SVPWM Simulation System. Diagrams for Blocks 1 to 7 are Shown in Figures 5.8 to 5.13.

Figure 5.8: Three-Phase Input Sinusoidal Voltages and Modulation Index are Detail for Block 1 in Figure 5.7.

4. In the fourth block, the switching time calculator is used to calculate the timing of the reference voltage vector. The inputs are the sector in which the voltage vector lies, the modulation index, the sampling time period of switching frequency, and $\cos \omega t$, and $\sin \omega t$. The duration time of the active and zero vectors are then calculated using

$$
\begin{bmatrix} T_a \\ T_b \end{bmatrix} = \frac{MI\sqrt{3}T_s}{\pi} \begin{bmatrix} \sin \frac{k\pi}{3} & -\cos \frac{k\pi}{3} \\ -\sin \frac{(k-1)\pi}{3} & \cos \frac{(k-1)\pi}{3} \end{bmatrix} \begin{bmatrix} \cos n\omega T_s \\ \sin n\omega T_s \end{bmatrix}.
$$

Figure 5.9: α, β Voltages and Modulation Index are Detail for Block 2 in Figure 5.7.
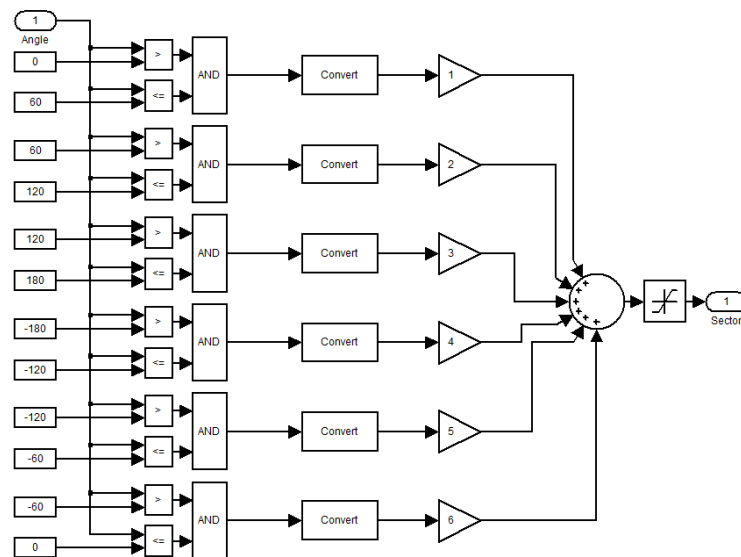
Figure 5.10: Detail for Block 3 in Figure 5.7.

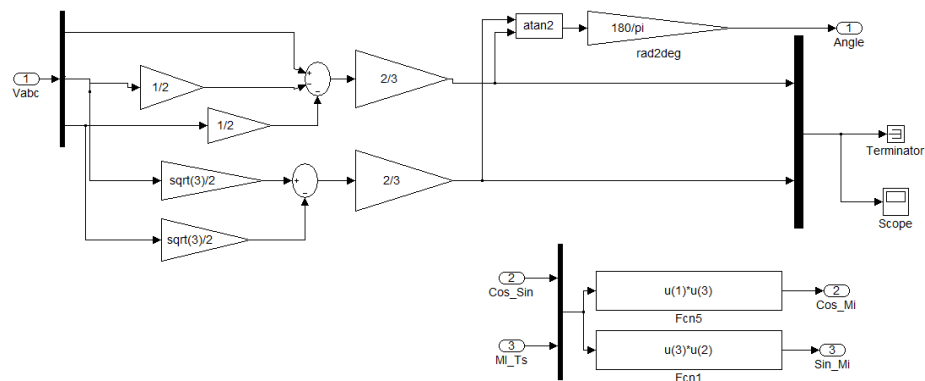In Figure 5.11, the time for the active and zeros vectors are arranged in the switching pattern sequence shown in Table 3.7. In the same block (Figure 5.11), we also have Sample & Hold blocks after sector T_a and T_b. The purpose of these blocks is to hold the values of T_a and T_b fixed during each T_{PWM} period [25].

5. The fifth block is a triangular generator used to produce a unit triangular waveform
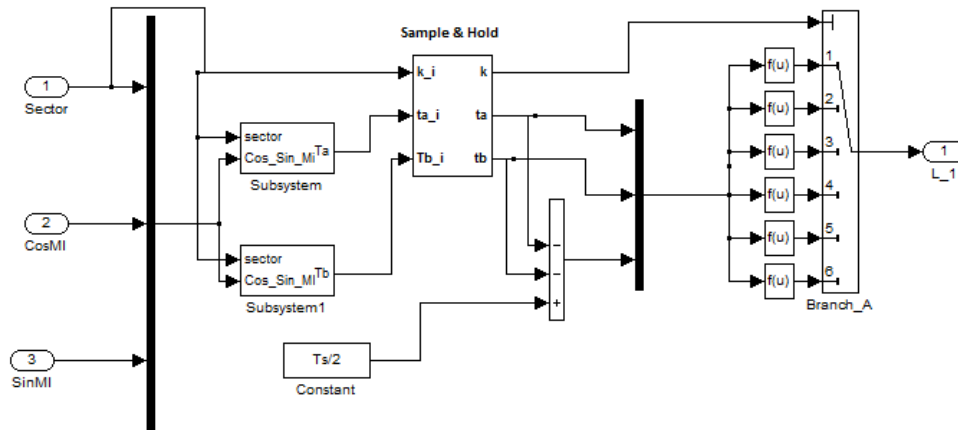
Figure 5.11: Switching Time Calculation is Detail for Block 4 in Figure 5.7.

at the PWM switching frequency.

6. The gate timing signals from the fourth block are compared with the triangular generator of fifth block, producing the outputs for the six switches of the inverter (Figure 5.12).
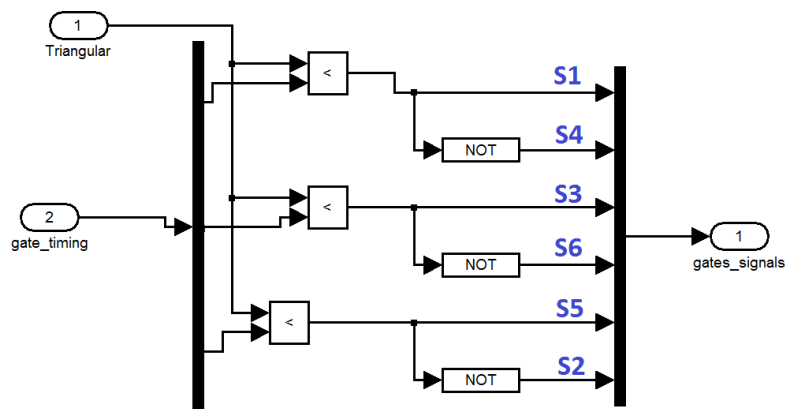

Figure 5.12: Timing Signals and Triangular Waveform Details for Block 6 in Figure 5.7.

7. The seventh block is built to simulate a voltage source inverter (Figure 5.13).

As seen in Figure 5.14, the inputs for the sixth block are the output time signals from
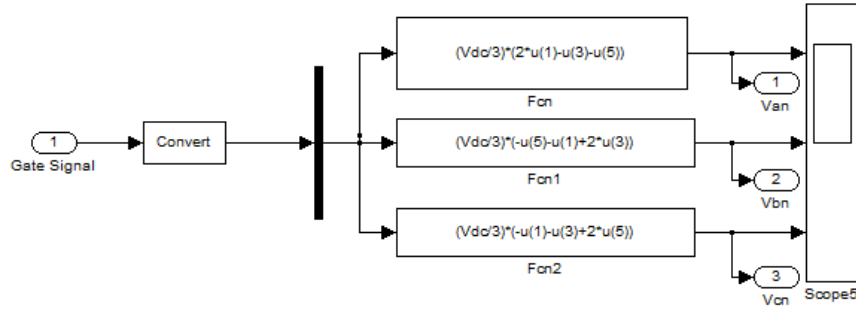
Figure 5.13: Inverter Output Signals to Neutral Voltages is Detail for Block 7 in Figure 5.7.

the fourth block and the triangular waveform is output from the fifth block. Figure 5.15 shows the pole voltages V_{ao}, V_{bo}, and V_{co} for Linear Modulation SVPWM. Due to the relationship between the DC bus voltage and the switching states of the output from the sixth block, we obtain the following PWM phase-to-neutral voltages:

$$V_{an} = \frac{V_{dc}}{3}(2S_1 - S_3 - S_5)$$
$$V_{bn} = \frac{V_{dc}}{3}(-S_1 + 2S_3 - S_5)$$
$$V_{cn} = \frac{V_{dc}}{3}(-S_1 - S_3 + 2S_5)$$

The simulation of the under-modulation of SVPWM is performed under the following conditions:
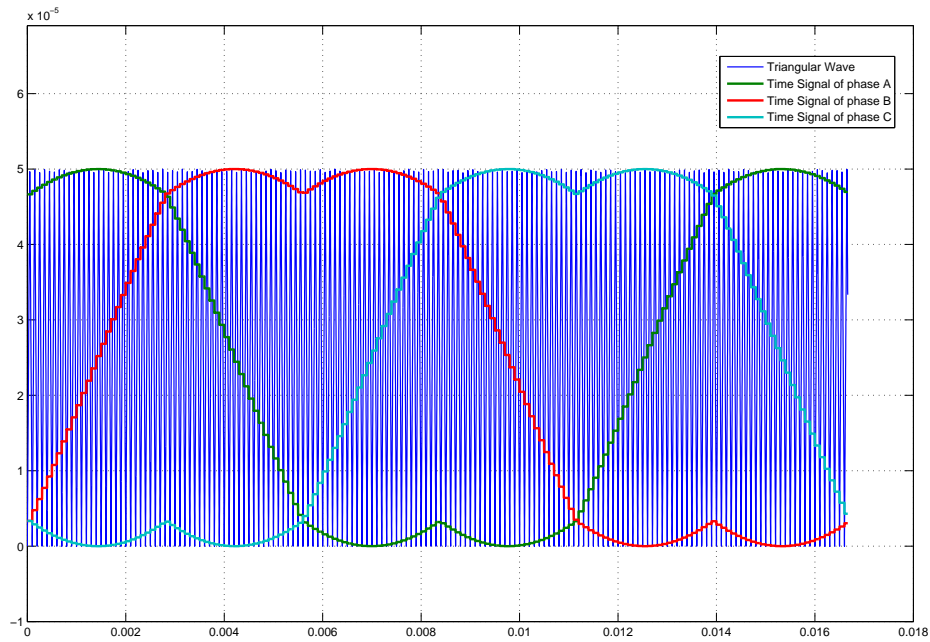
Figure 5.14: Filtered Timing Signals of Three-Phase and Triangular Waveforms in SVPWM.

$$V_{dc} = 300 \text{ V}$$

$$\text{Sampling time period} = 1/1800 \text{ Sec}$$

$$\text{Inverter frequency} = 60 \text{ Hz}$$

$$V_{ref} = \frac{300}{\sqrt{3}} \text{ V}.$$

Figure 5.16 shows the output voltage waveforms obtained from the SVPWM strategy. The modulation waveform of the seven-segment SVPWM has a saddle shape when passed through a low-pass filter (Figure 5.16) and its line-to-neutral voltages are sine waveforms because of the under-modulation PWM region (Figure 5.17). The maximum neutral voltages V_{an}, V_{bn}, and V_{cn} in Figure 5.18 is $V_{dc}/\sqrt{3}$ (173.2 Volts).
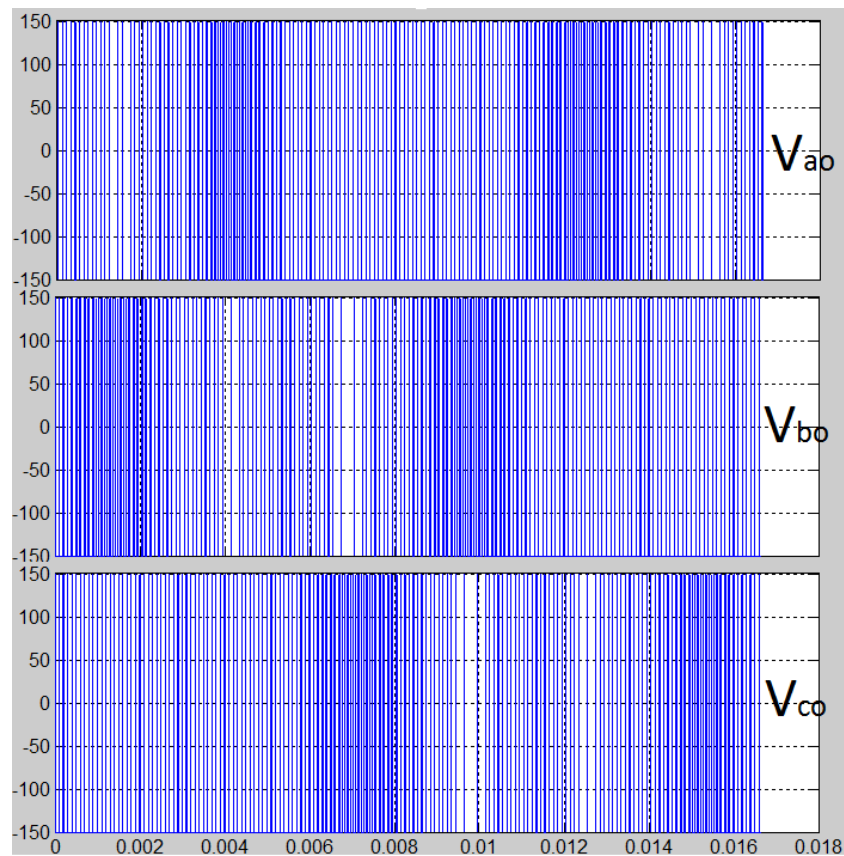
Figure 5.15: V_{ao}, V_{bo}, and V_{co} for Linear Modulation SVPWM.

5.5 Mode 1 in Over-Modulation of SVPWM

In the over-modulation region 1, additional calculations are required to compute the reference space vector. As mentioned before, there is a loss of fundamental voltage in the region where the reference vector exceeds the hexagon boundary. To compensate for this loss, the reference vector amplitude is increased in the region where the reference vector is inside the hexagon boundary. The magnitude of the reference vector is changed from the reference voltage vector to a modified reference voltage vector. A modified reference voltage trajectory proceeds partly on the hexagon and partly on the circle. When it remains on the circular part, the switching time of T_a, T_b, and T_0 are similar to the equations used
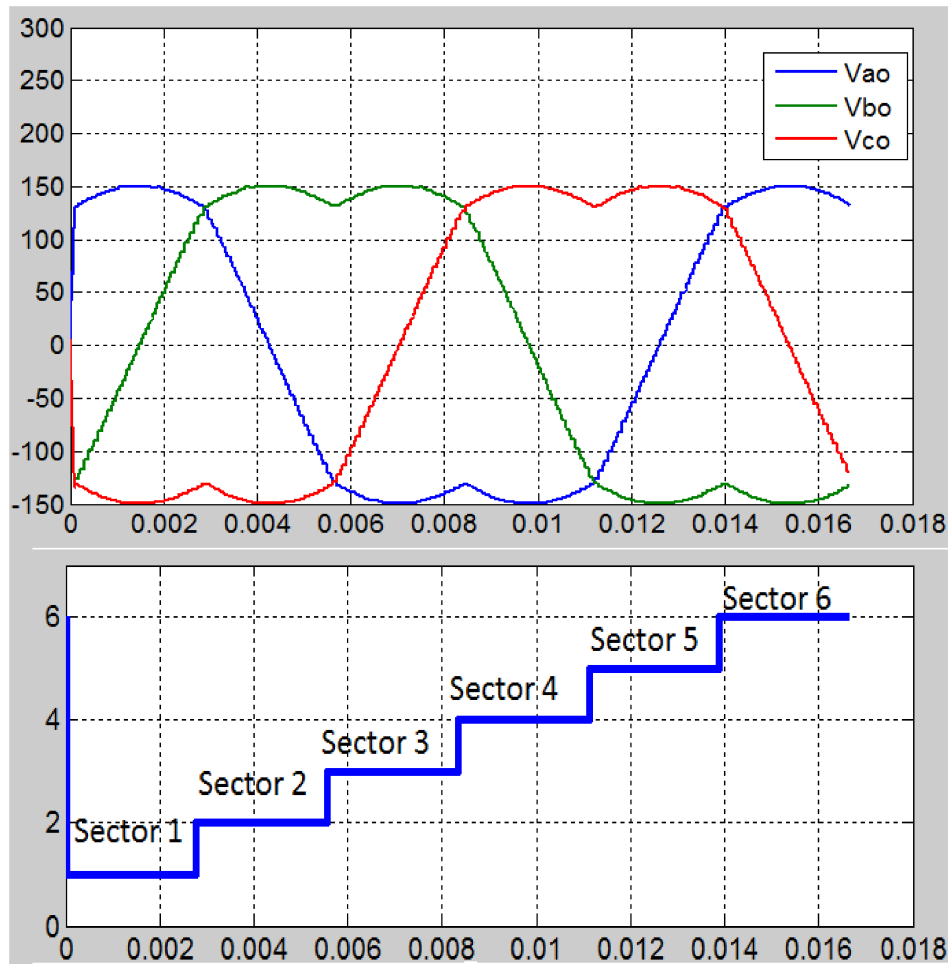
Figure 5.16: V_{ao}, V_{bo} and V_{co} for Linear Modulation SVPWM after Filtering.

for under-modulation. When the reference voltage vector passes outside of the hexagon, the value of T_0 is negative and meaningless. This problem is overcome by rescaling the duration times. Thus, $T_0'=0$, and T_a' and T_b' are the new time intervals shown in Table 4.1.

The simulation system model of the over-modulation region 1 of SVPWM is the same as that of the under-modulation SVPWM system except for the lookup table in first block and an added fourth block. The lookup table in the first block is the relationship between MI and the crossover angle, which is shown in Figure 4.2. For an added fourth block, the switches will be changed based on the duration T_0 of the zero state vectors.
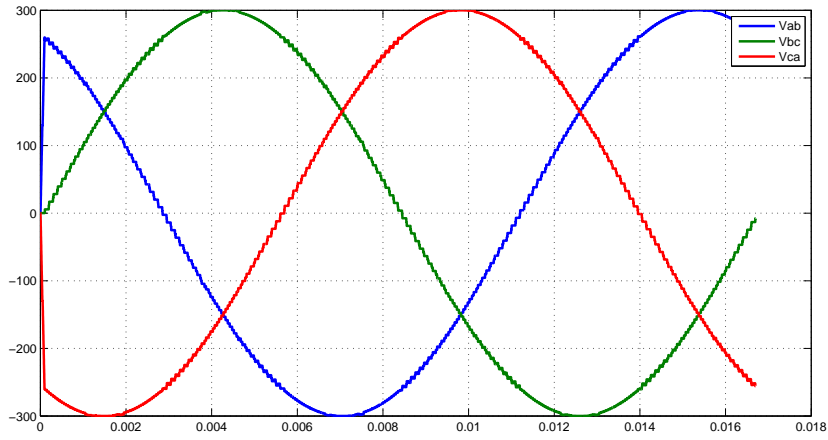
Figure 5.17: Line to Line Voltages of Linear-Modulation Region.
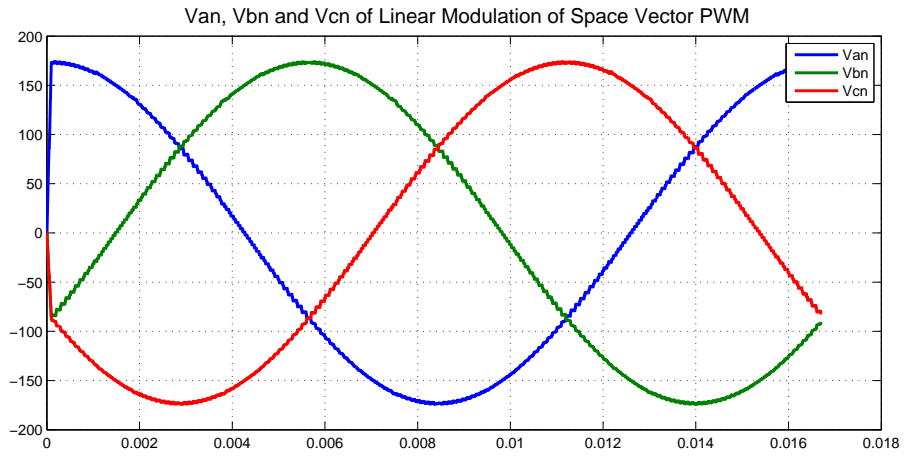
Figure 5.18: Neutral Voltages V_{an}, V_{bn}, and V_{cn} of Linear Modulation SVPWM after Filtering.

- When T_0 is greater than zero, the duration times T_0, T_a, and T_b shown in Table 3.5 are used.

- When T_0 is less than zero, the active duration times become T_a' and T_b', as shown in

Table 4.1.

Figure 5.19 shows the lookup table in the first block. Figure 5.20 shows the additional
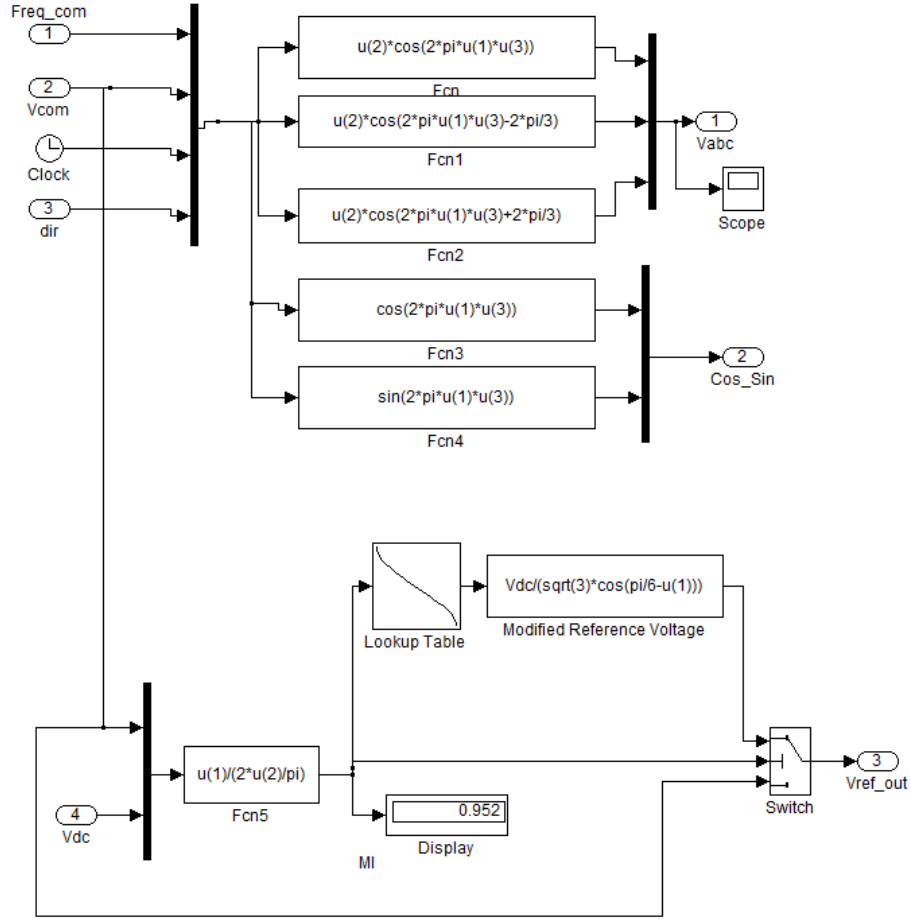
Figure 5.19: Detail of the Lookup Table in the First Block of SPVWM Over-Modulation Region 1.

block, which is a judgment condition for the over-modulation based on the sign of T_0. In red circle, if T_0 is negative, then T_a' and T_b' are used in the blue block.

As mentioned before, in the over-modulation region 1, the magnitude of the reference voltage vector is changed while the angle remains unchanged. This region ends when the reference voltage is traveling along the sides of the hexagon. The simulation results are

Figure 5.20: Detail of the Fourth Block of Space Vector PWM in Region 1.

presented to verify the effectiveness of this analysis. Figure 5.21 shows the output voltages

for region 1 of the over-modulation.

Compared to Figure 5.16, the phase voltage waveforms of Figure 5.21 do not have the

saddle waveform shape seen in the under-modulation SVPWM, but they stay at the limit

of the hexagon.

Figure 5.22 shows the neutral voltages V_{an}, V_{bn}, and V_{cn} in region 1 of the over-

modulation SVPWM after filtering. The voltage waveforms are no longer pure sine wave-

forms. Since the desired trajectory passes outside of the hexagon, the converter exceeds

its linear region of operation and enters the over-modulation region. Therefore, the syn-

thesized waveforms become distorted.

The low pass filter removes the high-frequency switching components, leaving the

triple order harmonics in the phase voltage waveforms. These harmonics do not affect

the line-to-line voltages [1]. As shown in Figure 5.23, the waveforms of the line-to-line

voltages V_{ab}, V_{bc}, and V_{ca} are less distorted compared to the neutral voltages in Figure 5.22.
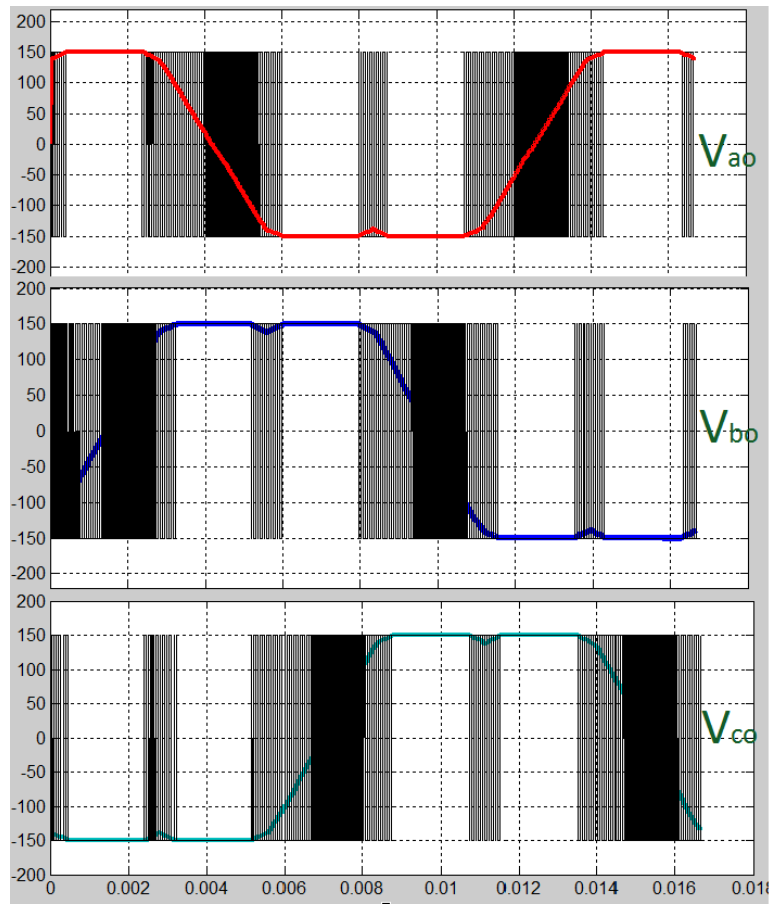
Figure 5.21: *V_ao*, *V_bo*, and *V_co* of Over-Modulation Region 1 before and after Filtering.
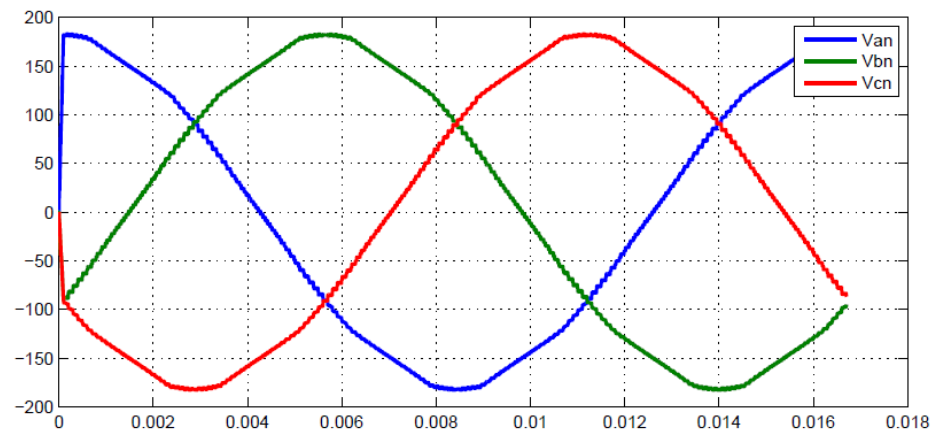
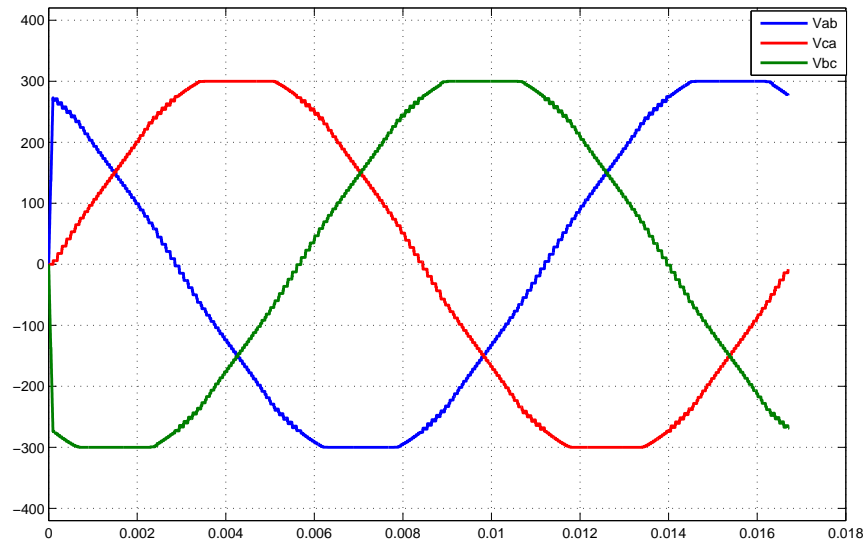Figure 5.22: Line-to-Neutral of Over-Modulation Region 1 after Filtering.

Figure 5.23: Line-to-Line Voltages of Over-Modulation Region 1 after Filtering.

CHAPTER 6

COMPARISON BETWEEN SPWM, THIPWM, AND SVPWM TECHNIQUES

6.1 Simulation Results

The simulation studies of Chapter 5 confirmed that the THIPWM and SVPWM techniques have a better DC bus voltage utilization than SPWM. As seen in Figure 6.1, the smaller circle represents the operating region of the SPWM technique and the larger inscribed circle represents the operating region of the SVPWM technique in the under-modulation region. In SVPWM, the length of each discrete space vector $\overrightarrow{V}_1$ through $\overrightarrow{V}_6$ is $2V_{dc}/3$. Each side of the hexagon midpoint is tangential to the inscribed circle. The largest possible magnitude of the reference voltage can be calculated as

$$MO = OL \times \cos(\frac{\pi}{6}) = \frac{2V_{dc}}{3} \times \frac{\sqrt{3}}{2} = \frac{V_{dc}}{\sqrt{3}}. \tag{6.1}$$

Since NM is perpendicular to OL, then

$$ON = OM \times \cos(\frac{\pi}{6}) = \frac{V_{dc}}{\sqrt{3}} \times \frac{\sqrt{3}}{2} = \frac{V_{dc}}{2}. \tag{6.2}$$

Thus, for SPWM, the smaller circle has a maximum magnitude of $V_{dc}/2$. It was already mentioned in Chapter 3 that the linear under-modulation region has a modulation index that approaches 90.7% for a maximum output fundamental of $V^*_{max} = (2/3)V_{dc} \times$

$\cos(\pi/6) = V_{dc}/\sqrt{3}$. The line-to-line voltage magnitude in linear SVPWM is thus equal to V_{dc}.

In SPWM, the maximum modulation index is 78.55%, the maximum output fundamental is 0.5 V_{dc}, and the maximum amplitude of the line-to-line voltage is $\sqrt{3}V_{dc}/2$. The line-to-line voltage of SVPWM is then increased by about:

$$\frac{V_{dc} - \frac{\sqrt{3}V_{dc}}{2}}{\frac{\sqrt{3}V_{dc}}{2}} \times 100 \approx 15.5\%. \tag{6.3}$$

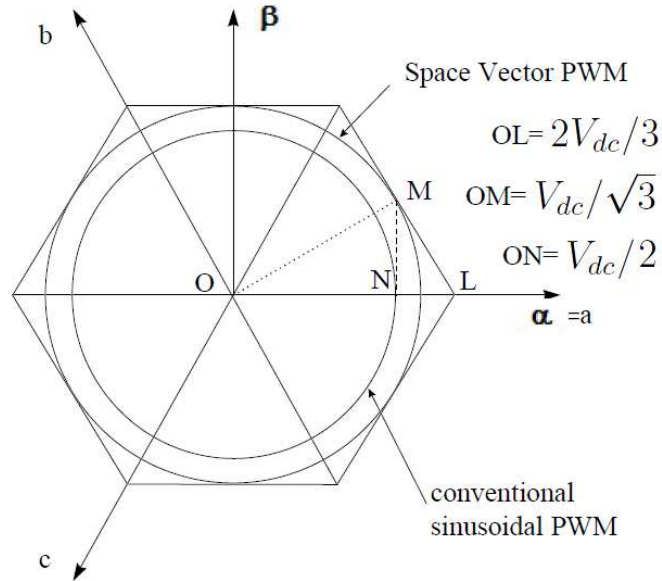Figure 6.1: Locus Comparison of Maximum Peak Voltage in SPWM and SVPWM [28].

From the simulation studies, the diagram in Figure 6.2 shows the evolution of the voltage reference vector $\vec{V}_{Ref}$ in the complex plane. The space voltage vector, which rotates with constant length and constant circular frequency, has the same features as that of a line-to-neutral phase voltage. The rotating space voltage vector is inside the

hexagon for under-modulation and between the inscribed circle of the hexagon and the circumscribed circle of the hexagon for over-modulation.
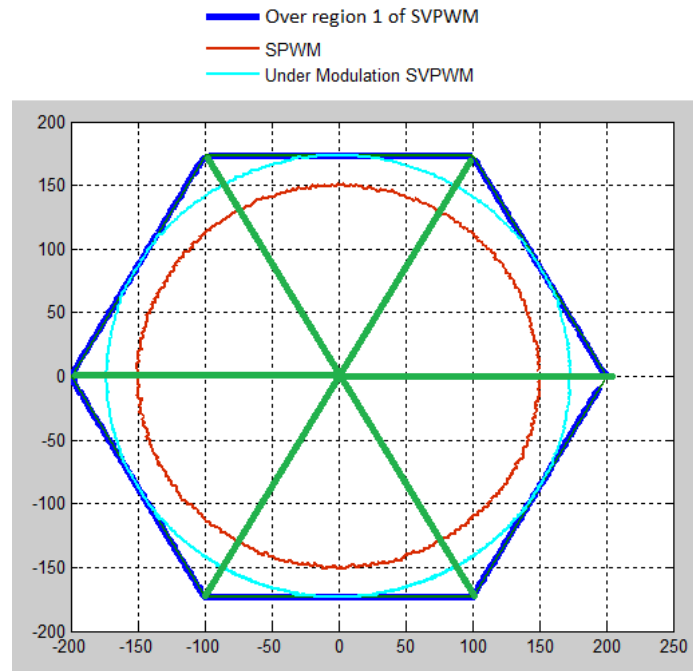
Figure 6.2: Loci of SPWM, SVPWM and Region 1 of SVPWM.

Figure 6.3 shows the locus of SPWM from the simulation results. When $\overrightarrow{V}_{ref}$ is desired to produce a balanced set of three-phase sinusoidal voltages, then the locus of $\overrightarrow{V}_{ref}$ is a circle inscribed inside the hexagon (Figure 6.4) when these space vectors are plotted on real and imaginary axes.

Figure 6.5 shows the maximum circle loci of THIPWM and under-modulation of SVPWM. They have the same radius.

In Figures 6.6 and 6.7, the locus of the space vector applied is partly circular and partly hexagonal. In the hexagon portion, only two active states are applied. The simulated
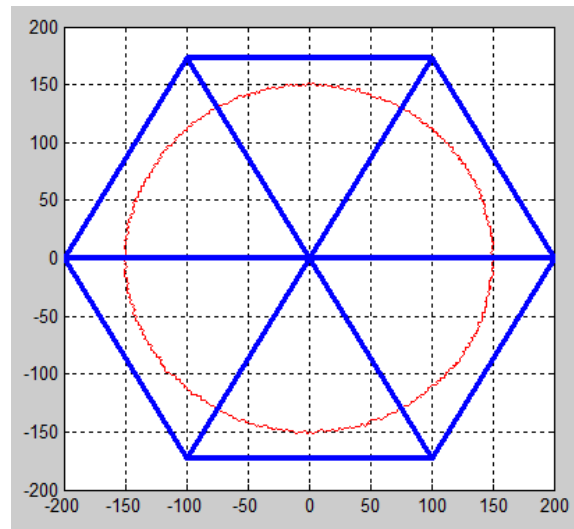
Figure 6.3: Locus of SPWM.
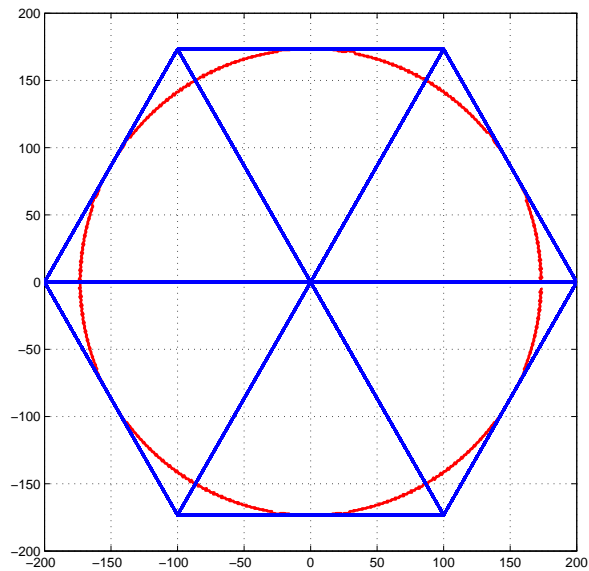
Figure 6.4: Locus of SVPWM in Linear Modulation Range.

results show that the over-modulation region 1 reported a modulation index that can reach to 0.952. This is an extension of about 5%, which is a significant improvement.
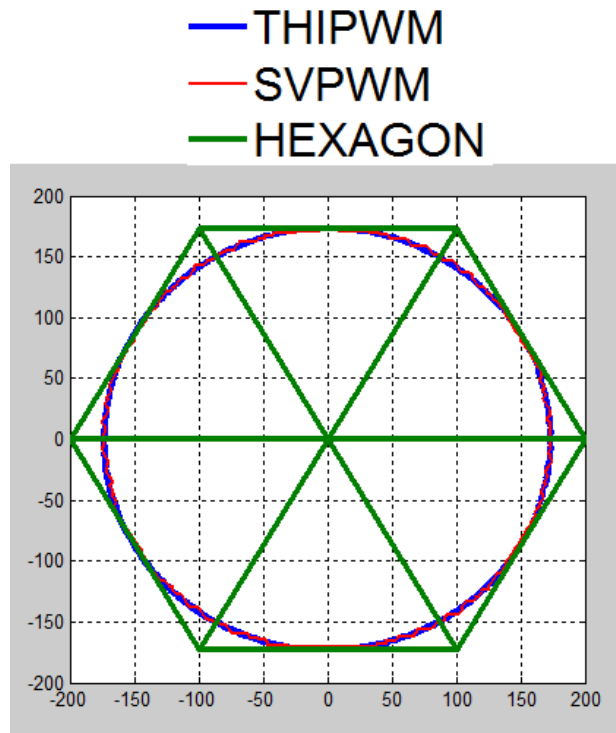
Figure 6.5: Loci of THIPWM and SVPWM.

6.2 Total Harmonic Distortion (THD) Comparison

In this section, the four different PWM techniques (SPWM, THIPWM, SVPWM in linear modulation range, and SVPWM in over-modulation range 1) are compared in terms of total harmonic distortion (THD). A Fast Fourier Transform (FFT) analysis in MATLAB is used to conduct the harmonic analysis. The harmonic spectrum of the inverter voltage waveforms of these techniques are presented with different modulation indices. The frequency modulation ratio in this analysis is 30 using a modulation frequency of 60 Hz and a carrier frequency of 1800 Hz. The results shown in tables and figures below include the first 50 harmonics. The sidebands frequency are positioned on both sides of the carrier frequencies with a frequency separation of $\pm \mu f_o$, where f_o is the frequency of
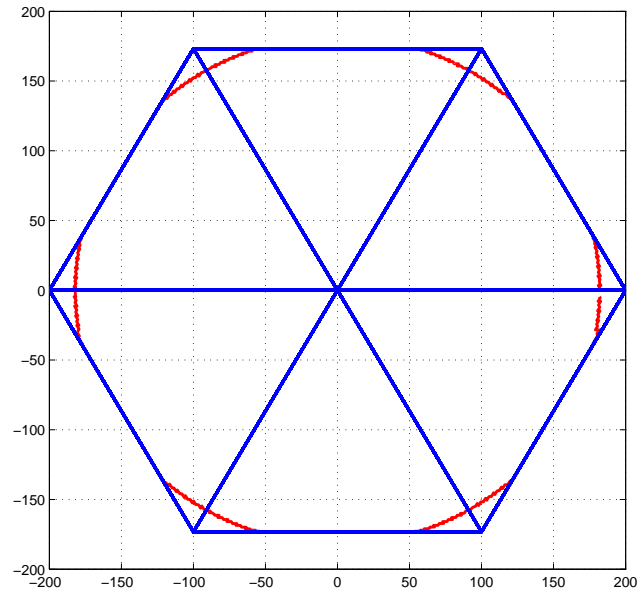
Figure 6.6: Locus of Over-Modulation Region 1 at a Cross Angle of 15 Degrees.
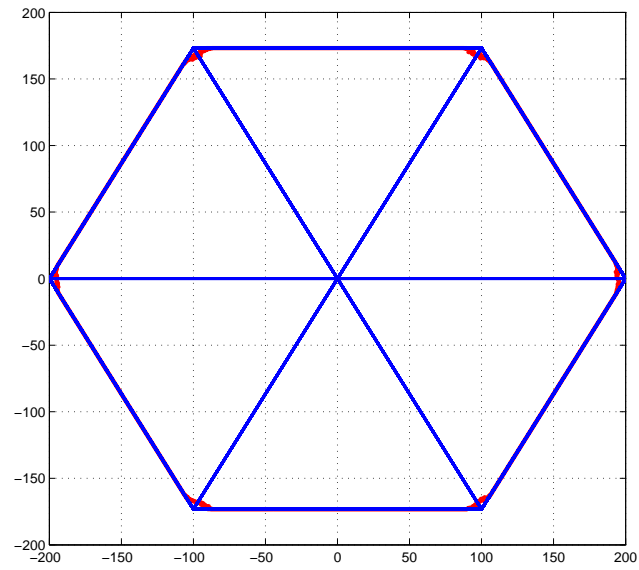
Figure 6.7: Locus of Over-Modulation Region 1 at a Cross Angle of 0 Degree.

the reference sinusoidal and μ is an integer that depends on the carrier harmonic frequency [26]. The harmonic number of individual sidebands can be found using the following

formula: $f_c \pm \mu f_o$, where f_c is carrier frequency.

V_{ao} of SPWM
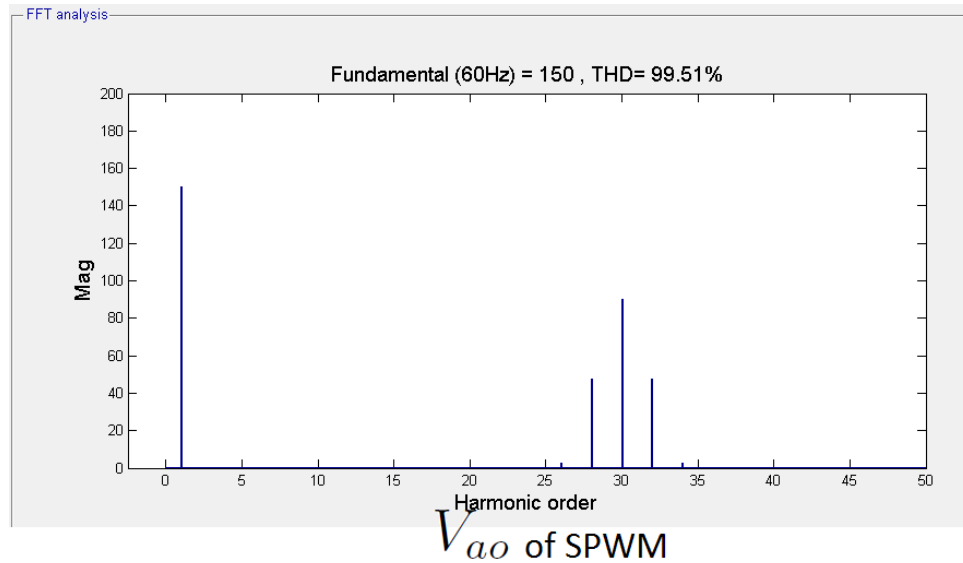
Figure 6.8: Spectrum of V_{ao} for SPWM.

Table 6.1: Pole Voltage V_{ao} in SPWM

MI	THD(%)	Fund	h26	h28	h30	h32	h34
0.733	113.3	140	2.06	42.73	101.34	42.7	2.06
0.7854	99.51	150	2.68	47.69	90.19	47.67	2.66

Figure 6.7 and Table 6.1 show the harmonic results for the pole voltage V_{ao} in the SPWM technique. As expected, we do not see a third harmonic in SPWM. Comparing the data of two different modulation indices in Table 6.1, we conclude that the higher modulation index has a lower THD (%).

Figure 6.8 and Table 6.2 show the harmonic results of the THIPWM technique. This technique has clearly increased the output voltage of the inverter compared to the SPWM technique. Thus, the third harmonics is presented and has increased phase and line-to-line voltages as well. As expected, the value of third harmonic in the V_{ao} is about one-sixth that of the fundamental voltage.
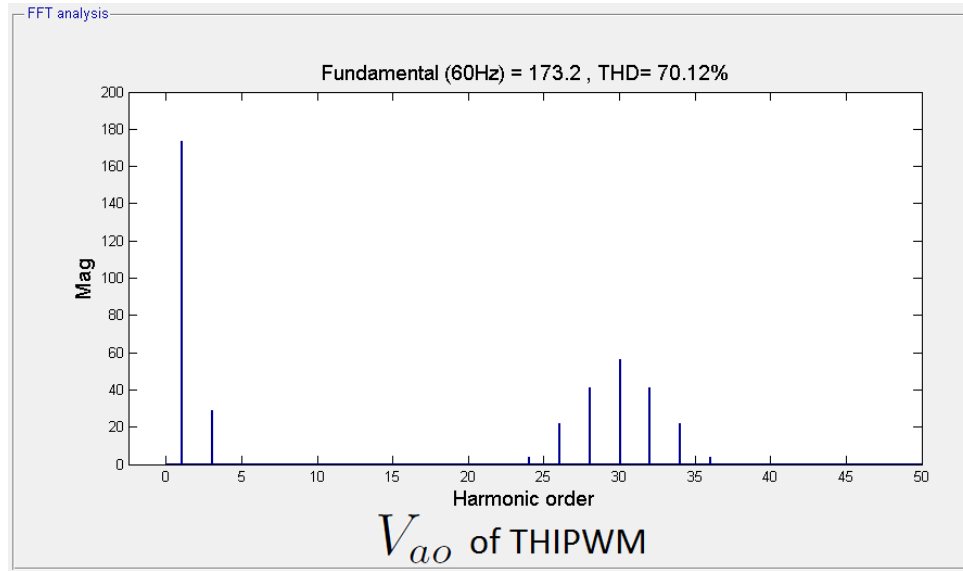
Figure 6.9: Spectrum of V_{ao} for THIPWM.

Table 6.2: Voltages V_{ab}, V_{an}, and V_{ao} in THIPWM

THD(%)	Fund	h3	h26	h28	h30	h32	h34	Voltages
51.76	300.08	≤ 1	37.56	71.42	≤ 1	71.42	37.49	V_{ab}
51.74	173.3	≤ 1	21.68	41.22	≤ 1	41.18	21.66	V_{an}
70.12	173.2	28.74	21.68	41.21	56.21	41.18	21.67	V_{ao}

Compared to SPWM, the values in 26th and 34th harmonic of THIPWM are very high and THD of THIPWM is significantly lower than for SPWM. The values of the 24th, and 36th harmonics are less than 5 Volts.

Table 6.3: Harmonics of V_{ao} in Under-Modulation range of SVPWM

MI	THD (%)	Fund	h3	h26	h28	h30	h32	h34
0.733	111.34	139.72	28.56	18.25	25.9	95.73	25.43	17.63
0.7854	97.38	149.7	30.61	20.48	29.03	83.53	28.57	19.85
0.806	92.03	153.71	31.41	21.40	30.30	78.53	29.84	20.76
0.9069	67.61	172.9	35.37	25.74	36.38	54.06	35.97	25.11

Figure 6.9 and Table 6.3 show the harmonic results of V_{ao} in the under-modulation
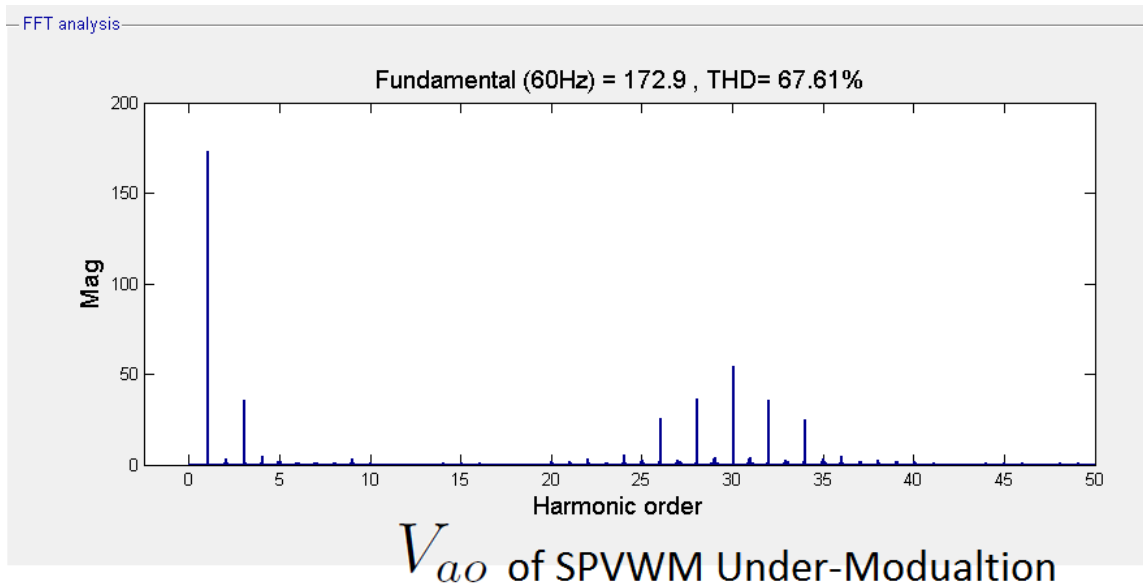
Figure 6.10: Spectrum of V_{ao} in The Under-Modulation Range of SVPWM.

region of SVPWM. In Table 6.3, there are four different modulation indices arranged in increasing order of magnitude. As in the SPWM technique, a lower modulation index has a higher THD (%). As can be seen from the figure, there are also a few values in the 22th, 24th, 36th, and 40th harmonic values but they are lower than 5 Volts.

Compared to SPWM with the same modulation index, the THD of SVPWM is slightly lower. The fundamental voltages (Fund) of both techniques are the same. Compared to THIPWM, the THD(%) of SVPWM (linear-modulation) is slightly lower than THIPWM and the value in the 3rd harmonic of SVPWM (under-modulation) is slightly higher than that in THIPWM. The fundamental voltages of both techniques are comparable.

Table 6.4: V_{ao} in Over-Modulation Region 1 of SVPWM

MI	THD(%)	Fund	h3	h26	h28	30	h32	h34
0.932	66.69	177.9	37.52	24.82	35.92	47.02	37.63	27.53
0.952	58.60	181.8	39.35	24.83	36.06	41.08	37.74	27.51

Fundamental (60Hz) = 181.8 , THD= 58.60%
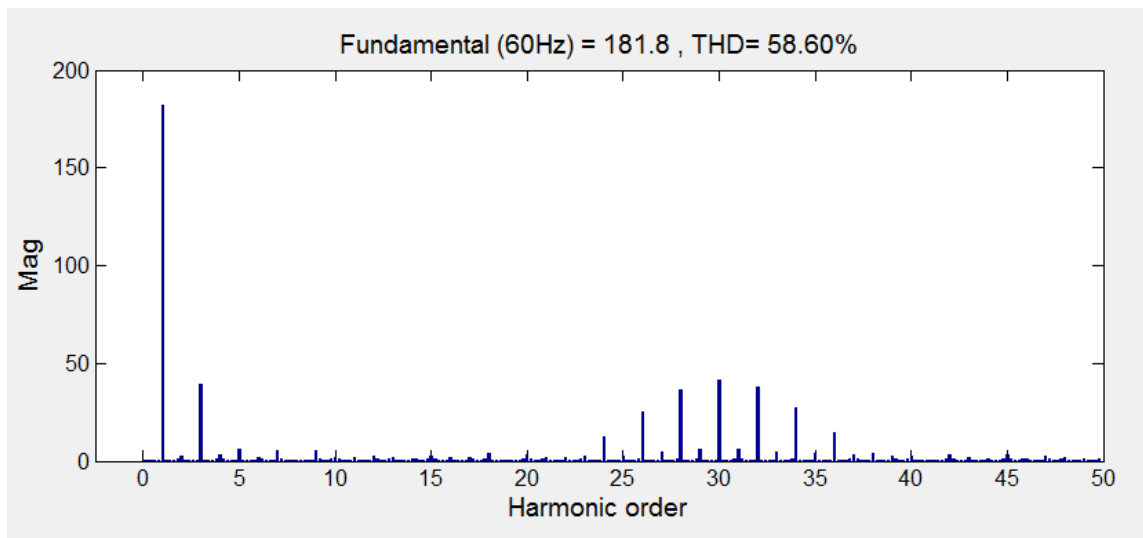
Figure 6.11: Spectrum of V_{ao} for SVPWM (Over-Modulation Region 1).

Figure 6.10 and Table 6.4 show the harmonic results of V_{ao} in the over-modulation region 1 of SVPWM. Overall, the spectrum of this technique is similar to the under-modulation of SVPWM. However, it has a higher fundamental voltage and a higher value of the 3rd harmonic. We also see additional harmonic values around the carrier frequency (30th harmonic) and a lower THD (%) with a higher modulation index.

Tables 6.5-6.10 show the harmonic results for V_{an} and V_{ab}. Tables 6.5-6.6 show the results of the SPWM technique. Tables 6.7-6.8 show the results of the SVPWM under-modulation technique. Table 6.8 shows the result of the SVPWM over-modulation region 1 technique. The line-to-line voltages are undistorted since the third harmonic components in the phase waveforms cancel out. The line-to-neutral voltages do not contain the third harmonic because this is a three-phase three-wire system. This means that there is no neutral connection to the wye-connected balanced load, and the triplen harmonic of the load currents must be zero.

Table 6.5: V_{ab} in the SPWM

MI	THD(%)	Fnd	h26	h28	h32	h34
0.733	75.32	242.50	3.58	73.97	73.99	3.57
0.7854	68.09	259.77	4.64	82.57	82.58	4.6

Table 6.6: V_{an} in the SPWM

MI	THD(%)	Fnd	h26	h28	h32	h34
0.733	75.32	140.01	2.07	42.71	42.71	2.06
0.7854	68.09	149.98	2.68	47.67	47.68	2.66

Table 6.7: V_{ab} in Under-Modulation of SVPWM

MI	THD (%)	Fnd	h26	h28	h32	h34
0.733	73.3	242	31.49	45.06	43.93	30.60
0.7854	66.01	259.3	35.24	50.50	49.36	34.44
0.806	63.14	266.24	36.89	52.70	51.58	36.01
0.9069	49.54	300	44.38	63.28	62.21	43.56

Table 6.8: V_{an} in Under-Modulation of SVPWM

MI	THD (%)	Fnd	h26	h28	h32	h34
0.733	73.29	139.7	18.52	25.88	25.44	17.62
0.7854	66	149.72	20.49	29.01	28.58	19.84
0.806	63.13	153.72	21.39	30.29	29.86	20.74
0.9069	49.51	172.9	25.74	36.37	35.97	25.10

Table 6.9: V_{ab} in Over-Modulation Region 1 of SVPWM

MI	THD(%)	Fnd	h26	h28	h32	h34
0.932	47.86	308	42.97	62.45	65.18	47.56
0.952	44.78	315	42.95	62.75	65.45	47.54

Table 6.10: V_{an} in Over-Modulation Region 1 of SVPWM

MI	THD(%)	Fnd	h26	h28	h32	h34
0.932	47.72	178	24.97	35.86	37.47	27.60
0.952	44.64	182.1	24.95	36.01	37.61	27.56

CHAPTER 7

CONCLUSION AND FUTURE WORK

7.1   Conclusion

This thesis has evaluated three different PWM techniques, namely SPWM, THIPWM, and SVPWM (in the linear modulation region and over-modulation mode 1). The contributions of the thesis are as follows:

- The thesis has provided a thorough review of the each techniques with a special focus on the operation of SVPWM in the under-modulation and over-modulation modes.

- In this thesis, Simulink models for all three techniques have been developed and tested in the MATLAB/Simulink environment. The SVPWM model is able to generate both the operation of the under-modulation region of SVPWM as well as the over-modulation region 1.

- The thesis discusses the advantages and drawbacks of each technique. Their simulation results are compared and analyzed by plotting the output harmonic spectra of various output voltages, and computing their total harmonic distortion (THD).

As seen from the simulation results, SVPWM and THIPWM have a superior performance compared to SPWM, especially in the over-modulation region of SVPWM. The SPWM technique is very popular for industrial converters. It is the easiest modulation scheme to understand and implement. This technique can be used in single-phase and three-phase

inverters.

The THIPWM technique operates by adding a third harmonic component to the sinusoidal modulating wave. It is possible to increase the fundamental by about 15.5% and, hence, allow a better utilization of the DC power supply. From the shape of the line-to-line voltages, the resulting flat-topped waveforms allow over-modulation with respect to the original SPWM technique.

The SVPWM technique can only be applied to a three-phase inverter and it increases the overall system efficiency. The SVPWM is used for controlling the switching of the machine side converter. Advantages of this method include a higher modulation index, lower switching losses, and less harmonic distortion compared to SPWM [27]. SVPWM research has been widespread in recent years making it one of the most popular methods for three-phase inverters because it has a higher fundamental voltage output than SPWM for the same DC bus voltage. The SVPWM is significantly better than SPWM by approximately 15.5%. However, the SVPWM technique is complex in implementation, especially in the over-modulation region.

The SVPWM technique has been deeply studied in the over-modulation region due to its performance benefits when compared to other modulation techniques. Numerous over-modulation algorithms have been proposed in the literature for the control of voltage source inverters [14,12,24]. The simulated results confirm that the over-modulation region 1 leads to a modulation index up to 0.952. This is an extension of around 5%, which is a significant improvement.

7.2   Recommendations for Future Work

There are couple of interesting topics suggested for future research:

- Further simulation studies should be performed in region 2 of over-modulation SVPWM

with neural networks and The Neural Network toolbox of MATLAB. Neural network implementation is very fast and can increase the switching frequency of power switches in the inverter.

- Many papers in the literature have reported that the dead time of space vector PWM has an influence on drive systems. To circumvent this problem, it is important to research how to compensate for the dead time effect in order to increase the performance of drive systems.

REFERENCES

[1] H. Salehfar, "DSP-Based Implementation of Vector Control of Induction Motor Drives," Taylor & Francis Group, LLC, 2005.

[2] R.K. Pongiannan, and N. Yadaiah, "FPGA Based Three Phase Sinusoidal PWM VVVF Controller," IEEE ICEES (International Conference on Electrical Energy Systems), pp. 34-39, 2011.

[3] A. Aktaibi, A. Rahman, and A. Razali, "A Critical Review of Modulation Techniques." Available from: http://necec.engr.mun.ca/ocs2010/viewpaper.php?id=13& print = 1.

[4] K.V. Kumar, P.A. Michael, J.P. John and S.S. Kumar, "Simulation and Comparison of SPWM and SVPWM control for Three Phase Inverter," Asian Research Publishing Network, Vol. 5, No. 7, pp. 61-74, July 2010.

[5] J.Y. Lee, and Y.Y. Sun, "A New SPWM Inverter with Minimum Filter Requirement," International Journal of Electronics, Vol. 64, No. 5, pp. 815-826, 1988.

[6] H. Quan, Z.Gang, C. Jie, Z. Wu, and Z. Liu, "Study of A Novel Over-modulation Technique Based on Space-Vector PWM," IEEE Computer Distributed Control and Intelligent Environmental Monitoring (CDCIEM), pp. 295-298, 2011.

[7] K. Zhou and D. Wang, "Relationship Between Space-Vector Modulation and Three-Phase Carrier-Based PWM: A Comprehensive Analysis," IEEE Transactions on Industrial Electronics, Vol. 49, No. 1, pp. 186-196, February 2002.

[8] W.F. Zhang and Y.H. Yu, "Comparison of Three SVPWM Strategies," Journal of Electronic Science and Technology of China, Vol. 5, No. 3, pp. 283-287, September 2007.

[9] A.W. Leedy, and R.M. Nelms, "Harmonic Analysis of a Space Vector PWM Inverter using the Method of Multiple Pulses," IEEE Transactions on Industrial Electronics, Vol. 4, pp. 1182-1187, July 2006.

[10] "Implementing Space Vector Modulation with the ADMCF32X," Analog Devices Inc., January 2000.

[11] B.K. Bose. Modern Power Electrics and AC Drives. Prentice-Hall, Inc., 2002.

[12] J. Holtz, W. Lotzkat, and A.M. Khambadkone, "On Continuous Control of PWM Inverters in the Over-modulation Range Including the Six-Step Mode," IEEE Transactions on Power Electronics, Vol. 8, No. 4, pp. 546-553, October 1993.

[13] J. Holtz, "On Continuous Control of PWM Inverters in Over-modulation Range Including the Six-Step, " IEEE Transactions on Power Electronics, Vol. 8, No. 4, pp. 546-553, 1993.

[14] D.C. Lee, "A Novel Over-modulation Technique for Space Vector PWM inverters," IEEE Transactions on Power Electronics, Vol. 13, No. 6, pp. 1144-1151, Nov. 1998.

[15] D.G. Holmes and T.A. Lipo. Pulse Width Modulation for Power Converters. John Wiley & Sons, Inc. 2003.

[16] A.M. Khambadkone, and J. Holtz, "Current Control in Over-modulation Range for Space Vector Modulation based Vector Controlled Induction Motor Drives," IEEE Industrial Electronics Society, Vol.2, pp. 1134-1339, 2000.

[17] J.A. Houldsworth, and D.A. Grant, "The Use of Harmonic Distortion to Increase the Output Voltage of a Three-Phase PWM Inverter," IEEE Transactions on Industry Applications, Vol. IA-20, No. 5, pp. 1124-1228, September-October 1984.

[18] M. Giesselmann, H. Salehfar, H.A. Toliyat, and T.U. Rahman, "Modulation Strategies," CRC Press LLC, 2002.

[19] A. Savulescu, "The Analysis and The Simulation of The SVM Generator Used for The Control of The Electric Drives with Asynchronous Motors," International Conference on Electromechanical and Power Systems, pp. 47-50, October 4-6, 2007.

[20] E. Hendawi, F. Khater, and A. Shaltout, "Analysis, Simulation and Implementation of Space Vector Pulse Width Modulation Inverter," International Conference on Application of Electrical Engineering, pp. 124-131, 2010.

[21] B. Wu. High-Power Converters and AC Drives. IEEE Press, John Wiley and Sons, Inc., 2006.

[22] MathWorks, 2010, SimPowerSystems, User's Guide.

[23] R. Cordero, and J.O.P. Pinto, "Relationship Between SPWM and SVPWM for Undermodulation and Overmodulation Modes Based on Modified Carrier Signal." Available from: http://www.labplan.ufsc.br/congressos/Induscon%202010/fscommand/ web/docs/I0275.pdf

[24] V.H. Prasad D. Boroyevich and R. Zhang, "Analysis and Comparison of Space Vector Modulation Schemes for Three-Leg and Four Leg Voltage Source Inverters," IEEE Applied Power Electronics Conference and Exposition, Vol. 2, pp. 864-871, February 1997.

[25] A. Oteafy, "How to Use a Sample & Hold Block after sector, duration time switching," Personal Communication.

[26] H. Patangia and D. Gregory, "A Harmonic Reduction Scheme in SPWM," IEEE Asia Pacific Conference on Circuits and Systems, pp. 1737-1740, 2006.

[27] C.U. Ogbuka and M.U. Agu, "A Generalized Rectified Sinusoidal PWM Technique for Harmonic Elimination," The Pacific Journal of Science and Technology, Vol. 10, No. 2, pp. 21-26, November 2009.

[28] Texas Instruments Europe, "Field Orientated Control of 3-Phase AC-Motors," Texas Instruments Incorporated, Literature Number: BPRA073, February 1998.